

# Development of a Pulsing Water System for the Fire Hose Method

A method of categorising erosion resistance of grass and clay

**Author:** M. Metselaar  
**Internal Supervisor:** V. Kitsikoudis  
**External Supervisor:** P. van Steeg



Assignment Period: 19 April - 30 June 2021  
Institution: University of Twente  
Host Company: Deltares  
Version: Final Report  
Date: 30th June 2021

# Development of a Pulsing Water System for the Fire Hose Method

A method of categorising erosion resistance of grass and clay

**M. Metselaar**

## Preface

This report is written as my bachelor thesis to conclude my Bachelor in Civil Engineering at the University of Twente. In this report "Development of a Pulsing Water System for the Fire Hose Method", the gravity valve and waterwheel concepts ability to create a pulsing stream is assessed. Theoretical understanding, analytical modelling and physical experiments are used as tools to ultimately give Deltares a recommendation on how to realise a non-powered pulsing water stream that meets requirements for their fire hose method.

I found the project very interesting, I had lots of freedom to use my own judgement to select and apply methods and skills to assess feasibility of the gravity valve and waterwheel concepts. Having the freedom to work on my own initiative helped me gain experience in the process of independent learning and research. It was also a valuable insight seeing how my small part of research fits into the bigger picture and contributes towards solving the overarching issue of flood defence in the Netherlands and the rest of the world.

Covid-19 has forced me to conduct the thesis project from home which was more challenging than I expected. This makes me even more grateful to my friends, colleagues and supervisors who helped and supported me during my Bachelor Thesis project. A special thank you goes to both my internal supervisor, Vasilis Kitsikoudis and my external supervisor, Paul van Steeg whose expertise and timely feedback really improved my report and learning process. I would also like to thank Deltares and Paul van Steeg for giving me the opportunity to work on this interesting project.

Meno Metselaar

Enschede, June 30, 2021

# Development of a Pulsing Water System for the Fire Hose Method

A method of categorising erosion resistance of grass and clay

M. Metselaar

## Summary

The Netherlands faces a colossal task to ensure all 3700 km of Dutch primary flood defences meet updated safety standards by 2050. New safety standards introduced in 2017 are now based on a combined failure probability of all defence failure mechanisms. One of the main failure mechanisms is wave overtopping. The extent of erosion due to wave overtopping is predominantly determined by the defence's grass cover erosion resistance. Current methods to determine grass cover erosion resistance are either large scale and expensive or small scale and fail to accurately consider the large scale properties of grass coverings. Deltares have developed the fire hose method, which aims to address the current technological shortfall by being able to classify grass cover erosion at low costs whilst considering large scale properties of grass covers. The method involves subjecting a grass cover section to continuous jet stream and assessing the damage caused after a certain period of time. Currently the jet stream is continuous however a pulsing stream is desired to better mimic the intermittent nature of overtopping waves.

Deltares desire a pulsing stream with a cycle time (time taken for one complete jet open and jet close period) in the range of one to six seconds and a ratio of jet open to jet close time in the range of four to twenty. The mechanism used to create this pulsing stream should also be non powered. The goal of this project is to assess the feasibility of two potential pulsing stream concepts to give Deltares confidence prior to committing resources at a large scale. The two studied concepts are the gravity valve and waterwheel concepts. The gravity valve concept uses water impulse to force open a freely swinging pivot valve, gravity will cause the valve to fall back into the stream obstructing it until the water impulse forces the valve open again, this continuous motion creates the desired pulsing stream. The waterwheel uses the jet to exert a force on the waterwheel blades causing it to rotate, as it rotates the blades intermittently block the jet stream creating the pulsing water stream.

The project aims to answer which pulsing water concept is most feasible according to theoretical understanding, how accurate is the theoretical description of the concept and what is the optimal setup for realisation of Deltares' full scale pulsing water system. The questions are answered using a structured methodology. Firstly theoretical understanding of both concepts is gained by applying mathematics and theories such as Newton's second law. Next the theory is applied to create analytical models of each concept, the models can help determine feasibility of the concepts and to what extent system parameters influence pulsing jet stream performance. Next, small scale physical experiments are performed to verify model predictions. Results of both theoretical models and physical experiments are compared and discussed to answer research questions and ultimately provide Deltares with a recommendation on how to realise a pulsing water system for the fire hose method.

Experimental results show that the gravity valve concept always experiences a dampening effect, the valve reaches a stationary condition and comes to rest constantly blocking the jet stream at an angle equal to the positive boundary (the boundary between valve - jet contact and no contact). This contrasts to model predictions that predicts a con-

tinuous swinging motion. The dampening could be caused by energy losses or that at some point during the swing cycle, the jet area only partially acts on the valve, reducing angular velocity and encouraging dampening. Both of which are not considered in the theory and analytical modelling. Future research should be conducted to determine exactly what causes the observed dampening effect. Nevertheless the gravity valve theory and analytical modelling studied can give valuable insight into how input parameters influence system performance and what additional measures are required to realise a working system.

Two theoretical methods were devised to explain and model the waterwheel system. Method 1 assumes the waterwheels spins at a constant angular velocity is equal to that of the jet velocity. Method 2 considers forces acting upon the system and uses the angular version of Newton's second law to derive equations for waterwheel angular acceleration, angular velocity and time with respect to the waterwheels rotational angle, theta. Method 2 better matches experimental results. Two non-dimensional parameters are identified for method 2 and their influence on the pulsing stream is explored. The first parameter is jet torque:waterwheel moment of inertia ratio. This parameter theoretically dictates waterwheel angular acceleration and thus cycle time. Lower ratios result in higher cycle times. The next parameter is the ratio between valve length and vertical distance from the wheel pivot to the jet stream ( $L:X$  ratio). Greater  $L:X$  ratios cause greater cycle times, except if  $L:X$  is sufficiently small (0.94 - 1.3), in which case greater cycle times are achieved due to such small waterwheel blade and jet contact time. Unfortunately both parameters are interconnected by  $X$  which also effects magnitude of jet stream torque, as a result the explicit effect of each parameter cannot be known.

The waterwheel concept is experimentally proven to create a lasting pulsing water stream and effects of  $L$ ,  $X$  and jet velocity at the nozzle ( $v_{noz}$ ) are well predicted by method 2. Deltares' desired jet open:close ratio between 4 - 20 can be achieved when with a  $L:X$  ratio between 0.943 and 0.991. This holds for when the jet nozzle angle is 20 degrees to the horizontal. Higher jet nozzle angles values will reduce the jet open:close ratios. Cycle times are seen to be in the order of 0.1 seconds, both experimentally and theoretically. This is well below Deltares' desired cycle time of 1-6 seconds. Therefore it is recommended that a braking system is devised to increase cycle times. A primitive frictional braking system was tested experimentally and achieved a cycle time increase of 34% thus proving braking system potential. It is unknown however whether braking systems can achieve large cycle time increases from 0.1 to 6 seconds. Surprisingly experimental data suggested that waterwheel moment of inertia had no effect upon cycle time. This contradicts method 2's theory in which moment of inertia is decisive in determining angular acceleration and thus cycle time. If moment of inertia appears to be redundant in influencing cycle time, waterwheel method 2 cannot be used to predict cycle times. More experiments should be performed on a wider range of waterwheel moment of inertia's to determine whether moment of inertia is influential.

## Contents

<b>1</b>	<b>Introduction</b>	<b>7</b>
1.1	Problem Description . . . . .	8
1.2	Research Objective . . . . .	9
1.3	Research Questions . . . . .	10
<b>2</b>	<b>Theoretical Understanding</b>	<b>11</b>
2.1	Gravity Valve Theory . . . . .	11
2.2	Waterwheel Theory . . . . .	13
2.2.1	Method 1: Jet Velocity Assumption . . . . .	15
2.2.2	Method 2: Force Considerations . . . . .	16
<b>3</b>	<b>Analytical Model Development</b>	<b>17</b>
3.1	Gravity Valve Model Development . . . . .	17
3.2	Waterwheel Model Development . . . . .	20
<b>4</b>	<b>Experimental Procedure</b>	<b>22</b>
4.1	Gravity Valve Experimental Set-up . . . . .	22
4.2	Waterwheel Experimental Set-up . . . . .	24
<b>5</b>	<b>Results</b>	<b>26</b>
5.1	Gravity Valve Results . . . . .	26
5.1.1	Gravity Valve Model Results . . . . .	26
5.1.2	Gravity Valve Experiment Results . . . . .	29
5.2	Waterwheel Results . . . . .	31
5.2.1	Waterwheel Analytical Model Results . . . . .	31
5.2.2	Waterwheel Experiment Results . . . . .	33
<b>6</b>	<b>Discussion</b>	<b>37</b>
6.1	Gravity Valve Discussion . . . . .	37
6.2	Waterwheel Discussion . . . . .	38
<b>7</b>	<b>Recommendation to Deltares</b>	<b>40</b>
<b>8</b>	<b>Conclusion</b>	<b>41</b>
	<b>Appendices</b>	<b>44</b>
<b>A</b>	<b>Gravity Valve Theory Calculations</b>	<b>44</b>
A.1	Phase 1: Only Weight Force Acting . . . . .	45
A.2	Phase 2: Jet Force and Weight Force Acting . . . . .	46
A.3	Phase 3: When theta is negative . . . . .	47
<b>B</b>	<b>Moment of Inertia Calculations</b>	<b>48</b>
<b>C</b>	<b>Waterwheel Theory Calculations</b>	<b>50</b>
C.1	Method 1: Jet Velocity Assumption . . . . .	50
C.2	Method 2: Force Considerations . . . . .	52
<b>D</b>	<b>Gravity Valve Matlab Script</b>	<b>54</b>
<b>E</b>	<b>Waterwheel Matlab Script</b>	<b>61</b>
<b>F</b>	<b>Impression of the Tested Braking System</b>	<b>64</b>
<b>G</b>	<b>Jet Impact Velocity Using Bernoulli</b>	<b>65</b>

## List of Figures

1	Illustration of the studied water driven gravity valve concept (above) and waterwheel concept (below). . . . .	9
2	Schematic image showing all forces and variables influencing the gravity valve system. . . . .	11
3	Demarcation of the gravity valve's swing cycle into three phases and six steps. . . . .	12
4	Schematic image showing all forces and variables influencing the waterwheel system. . . . .	14
5	Demarcation of the gravity valve's swing cycle into three phases and six steps. . . . .	17
6	How initial theta, angular velocity and time values are found at each of the six gravity valve swing cycle points. . . . .	18
7	Flow chart showing how gravity valve MATLAB model functions. . . . .	19
8	Flow chart showing how waterwheel MATLAB model functions. . . . .	21
9	Impression of the physical experimental setup used to test the gravity driven pivot valve theory. . . . .	22
10	Impression of the physical experimental setup used to test the waterwheel theory. . . . .	24
11	Effect of jet : weight torque ratio on gravity valve's cycle time and open : close ratio. . . . .	28
12	Effect of valve length : X ratio on gravity valve's cycle time and open : close ratio. . . . .	28
13	Effect of valve length : OA ratio on gravity valve's cycle time and open : close ratio. . . . .	28
14	Effect of $\theta_{start}$ on gravity valve's cycle time and open : close ratio. $\theta_{start}$ ranges from the positive boundary (0) to pi/2 (1). . . . .	28
15	Experimental results compared against model predictions for gravity valve test 1.1 with three different applied $v_{noz}$ values. . . . .	29
16	Experimental results compared against model predictions for gravity valve test 2 with different chosen X values. . . . .	30
17	Effect of $v_{noz}$ on system cycle time and open : close ratio for waterwheel method 1. . . . .	32
18	Effect of length : X ratio on system cycle time and open : close ratio for waterwheel method 1. . . . .	32
19	Effect of jet torque : moment of inertia ratio on system cycle time and open : close ratio for waterwheel method 2. . . . .	32
20	Effect of length : X ratio on system cycle time and open : close ratio for waterwheel method 2. . . . .	32
21	Experimental results of test 1.1, a two bladed waterwheel with three different chosen X values. Results are compared against method 1 (jet velocity model) and method 2 (force model) predictions. . . . .	34
22	Experimental results of test 1.2, a two bladed waterwheel with three different water wheel moment of inertia values. Results are compared against method 1 (jet velocity model) and method 2 (force model) predictions. . . . .	35
23	Experimental results of test 1.3, a two bladed waterwheel with three different L values. Results are compared against method 1 (jet velocity model) and method 2 (force model) predictions. . . . .	35
24	Experimental results of test 1.4, a two bladed waterwheel with three different applied $v_{noz}$ values. Results are compared against method 1 (jet velocity model) and method 2 (force model) predictions. . . . .	36

25	Experimental results for waterwheel with three blades with and without brake system applied. Results are compared against method 1 (jet velocity model) and method 2 (force model) predictions. . . . .	36
26	Illustration of the gravity valve concept (above) and the waterwheel concept and its defined $L$ and $X$ parameters (below). . . . .	42
27	Effect of blade length : $X$ ratio on system cycle time and open : close ratio for waterwheel method 2. . . . .	42
28	Trigonometric relations used to derive both the gravity valve's positive and negative boundaries. . . . .	44
29	Three different configurations of valve or blade mass distribution depending on the chosen value of $OA$ . . . . .	49
30	Trigonometric relations used to calculate the angle during which the jet stream is blocked by the waterwheel, $\theta_j$ . . . . .	50
31	The three phases defined as a waterwheel blade blocks the jet stream. . . . .	51
32	Impression of the waterwheel's tested frictional braking system. . . . .	64
33	Trigonometric relations used to determine $h_1$ as a function of theta to complete Bernoulli's equation. . . . .	65

**List of Tables**

1	Overview of the three defined gravity valve swinging phases and their subsequent steps. . . . .	12
2	Overview of all equations used by the gravity valve model for each phase and step. . . . .	17
3	Three equations used to determine waterwheel motion when in contact with the jet stream. . . . .	20
4	Overview of the 33 physical gravity valve tests conducted using four different valve types. . . . .	23
5	Overview of the 21 physical waterwheel tests conducted. . . . .	25
6	Overview of the baseline parameters used for each gravity valve model test. . . . .	27
7	Overview of the baseline parameters used for each waterwheel model test. . . . .	31
8	Overview of $v$ and $OB$ values as well as theta boundaries for each of the three defined waterwheel jet contact phases. . . . .	51
9	Overview of $\tau_{F_n}$ values as well as $\theta$ boundaries for each of the three defined waterwheel jet contact phases. . . . .	52

## 1 Introduction

The Netherlands has had a rich history in flood defence. Roughly 60% of the country is prone to flooding from either the North sea coast, the rivers Rhine and Meuse or the great lakes (Rijkswaterstaat., 2012). Historically, the country’s flood defence policy has largely been shaped in response to disasters. Arguably none more so than the 1953 flood disaster which triggered the introduction of scientific methods and recommended flood defence safety standards expressed as exceedance probabilities (Voorendt, 2015). Exceedance probability is a safety standard in which a flood defence must resist overtopping for a high water level with a certain return period. More recently in 1993 and 1995 high water levels caused flooding on the Meuse and mass evacuation around the Rhine (Jak and Kok, 2000). Coupled with increasing climate change awareness, growing populations and increasing economic damage potential, the systems limited capacity was recognised and the issue of flood defence was once again a political priority (Wesselink et al., 2007).

The Netherlands consequently switched to a risk based flood safety approach which considers probability and consequences of failure (van der Most et al., 2014). Since 2017 new flood defence standards are based on a combined failure probability of all failure mechanisms rather than on exceedance probabilities which was dominated by overtopping mechanisms (Voorendt, 2015). Specific dike stretches are also now given their own safety standard depending on the consequences of their failure. Previously entire dike rings had the same safety standard. A lot of work is required as all 3700km of Dutch primary flood defences must comply with these new standards by 2050 (van Alphen, 2015). On top of that, the Water Act currently requires evaluation of each flood defence once every 12 years to check whether they still meet safety standards (Rijkswaterstaat., 2010).

One of the main flood defence failure mechanisms to be evaluated in these new standards is wave overtopping (van Bergeijk et al., 2020). Waves overtopping the flood defence inflict high flow velocities on the crest and landward slope which can lead to significant erosion (van Bergeijk et al., 2020). Grass cover condition is fundamental in determining the extent of the erosion. Grass cover dikes are employed throughout the world in places such as US and China and are increasingly recognised for their ecological value (van Bergeijk et al., 2020). In fact, Trung et al., (2016) state that many simulator tests have revealed that the relationship between the shear strengths of a subsoil and the grass turf predominantly determines how damage happens to a dike slope. This is reinforced by van Bergeijk et al., (2021), whose model observes a failure probability increase by a factor of up to 1000 when comparing dikes with poor grass covers to those with good grass covers.

Current methods to predict damage of grass mats and dike erosion include, among others, the Grass Erosion Model (GEM) and the Cumulative Overload Method (COM). The latter is currently used by the Dutch government as the standard tool to assess dike failure due to wave overtopping (van Bergeijk et al., 2020). COM is based on 50 experiments conducted between 2007 and 2014 on Dutch and Belgian dikes using an overtopping simulator (Hoffmans et al., 2018). The model predicts damage provided the load of the overtopping wave and the critical flow of the grass cover is known (Hoffmans et al., 2018). A grass cover’s critical flow is defined as the flow velocity threshold in which erosion occurs (Warmink et al., 2020).

The determination of grass cover erosion resistance in the form of, among others, critical velocity is clearly vital to determine erosion damage and thus failure probabilities for wave overtopping. Determining a representative erosion resistance is challenging due to the inhomogeneous nature of grass covers and the influence of transitions (change in material, geometry or roughness) (Warmink et al., 2020). Large scale research methods such as the Delta flume or the aforementioned overtopping simulator have been devised to determine grass cover erosion resistance however they are very immobile and expensive. On the other hand smaller scale methods such as the jet erosion test (JET) or the pocket erodometer test (PET) fail to provide dependable results and information on the large scale properties of grass coverings.

In an effort to solve this issue, Rijkswaterstaat commissioned Deltares in the context of the knowledge of primary processes (KPP) project strengthening flood risk research, to assess feasibility of creating one workable device that can account for larger scale grass cover characteristics and classify erosion resistance, preferably in terms of critical velocity for direct compatibility with the COM. The resulting concept is the so called firehose method as outlined in the report of van Steeg and Mourik (van Steeg and Mourik, 2020). The method involves subjecting a dike section to a continuous water stream and assessing the damage caused after a certain period of time. It cannot directly measure erosion resistance however it may be able to classify it. Ideally the method could be used in conjunction with an existing classification such as the one proposed by Briaud et al., (2019) which relates erosion rate (mm/hr) to applied water velocity (m/s). However it appears the existing Briaud classification is based on small scale tests and is not accurate enough; all Dutch grass covers fall within the same category. A new classification method for the Fire Hose Method would be required and could offer improved classification accuracy for grass covers. The Fire Hose Method’s primary intended application is testing irregularities in grass covers which are likely weak spots exposed to higher hydraulic loads such as the landward toe or transition areas. The quick erosion resistance classification is extremely valuable in contributing towards assessment of failure probabilities due to wave overtopping for all primary flood defences in the Netherlands. Currently the fire hose’s water stream is continuous however it is desirable for it to be pulsing as this better mimics the wave action that erodes dikes. Theoretical understanding of achieving this “pulsing system” must be understood before it can be implemented and tested.

### 1.1 Problem Description

After devising and constructing the so called “Fire Hose Method”, Deltares looked into the practicality of creating a pulsing water stream. Solutions using powered mechanical parts to block the stream were ruled out with an unpowered solution being preferred. With limited time and budget remaining research could not be done and instead a quick physical test was made based on the concept of a gravity driven pivot valve, the set up consisted of a water hose and a swinging valve both held by a wooden frame as illustrated in Figure 1. The concept intends to work by using the water impulse to force open the freely swinging pivot valve. Gravity will cause the valve to fall back into the stream obstructing it until the water impulse forces the valve open again. This continuing motion causes the pulsing water stream. The quick physical test did not work because the pivot valve found an equilibrium position within the water stream and stopped oscillating thus not creating the desired pulsing stream.

An alternative concept is based upon a waterwheel, the water stream exerts a force upon the wheel blades causing the wheel to rotate. The blades intermittently interrupt the water stream creating the pulsing water stream as illustrated in Figure 1. Currently, a theoretical understanding of a non-motorised pulsing water system is unknown to Deltares. Theory must be understood and verified on a small scale before Deltares can commit resources to its larger scale construction to ultimately test the performance of the pulsing fire hose method.

Within this project the term “concept” means the abstract idea of the mechanism used to create the pulsing water stream. In this project only the “gravity valve” and “waterwheel” concepts will be researched. The term pulsing water “system” refers to all constituting parts and values that make up the pulsing water mechanism, this includes configurations of the water stream, nozzle and gravity valve or waterwheel dimensions and weight distributions. All of which interact and must have specific values to achieve a pulsing water stream with desired characteristics.

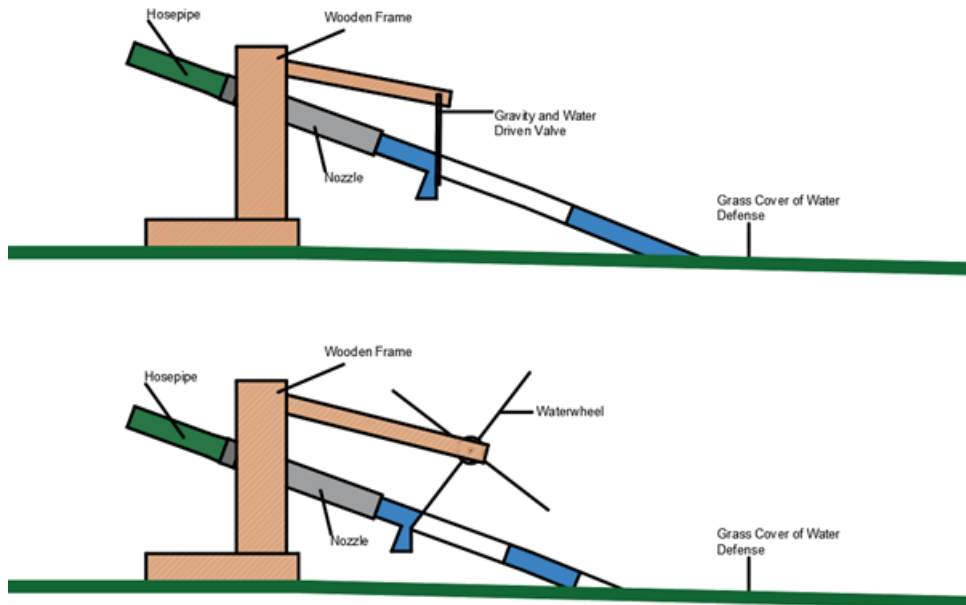


Figure 1: Illustration of the studied water driven gravity valve concept (above) and waterwheel concept (below).

## 1.2 Research Objective

Following from the problem description the research objective is to examine the gravity valve and waterwheel's feasibility of creating a non-powered pulsing water stream for the full scale fire hose method and to provide Deltares with a recommendation for its future realisation.

Theoretical understanding of the concepts will be achieved by applying theories such as Newton's Laws of motion. Both concepts will be modelled in MATLAB to predict how different system input parameters effect the pulsing stream performance. For example by determining the relationship between water force and performance indicators like cycle time and jet open:close ratio. Physical experiments are performed for both concepts, the gathered experimental data can be used to verify, improve and calibrate the theory and models. Using the model and experimental results a recommendation will be made to Deltares for the theoretical upscaling of the chosen concept for use in their larger scale fire hose method experiments. This project focuses on the theoretical understanding of such concepts and will not give insight into their design and technical construction. It is possible this research project's recommendation is that neither concept is viable, which is nevertheless a valuable conclusion for Deltares.

Encapsulating everything above into a single sentenced research objective leads to:

**To assess the feasibility of a non-powered pulsing water system for Deltares' Fire Hose Method by understanding, modelling, practically verifying and scaling up the theoretical relations behind it.**

This research project will provide Deltares with a recommendation of which pulsing water concept to choose and how to realise the system at full scale. This will enable Fire Hose Method experiments to be conducted with a pulsing water stream to better mimic the intermittent nature of wave overtopping erosion. This will hopefully cement the Fire Hose Method as a valuable world-wide method for grass cover erosion resistance classification.

### 1.3 Research Questions

In order to provide Deltares with a recommendation on how to realise a non-powered pulsing water system, three main research questions have been formulated.

1. Which pulsing water concept is the most feasible according to theoretical understanding?
  - a Is the gravity valve concept feasible? – Select and apply theoretical principles to explain the concept, identify influential variables, state assumptions and predict the effect of system parameters on pulsing performance using a MATLAB model.
  - b Is the waterwheel concept feasible? – Select and apply theoretical principles to explain the concept, identify influential variables, state assumptions and predict the effect of system parameters on pulsing performance using a MATLAB model.
2. How accurate is the modelled description of the chosen pulsing water system?
  - a What are the model uncertainties and how should they be addressed? – Determine the weak aspects (simplifications, parameter uncertainty upscaling uncertainty) of the analytical model. Use a calibration parameter to account for these uncertainties.
  - b How does the model compare to experimental results? – Conduct a physical experiment to determine model accuracy in water stream cycle time and jet open : close ratio predictions. Use the experiment to calibrate the model.
3. What is the optimal set up for realisation of Deltares’ full scale pulsing water system and what should be considered regarding the reliability of upscaled predictions?
  - a What is the optimal set-up for realisation of Deltares’ full scale pulsing water system? – Determine based on the modelled effect of system parameters, which setup would be most desirable to ensure a working pulsing water system at full scale water stream values. The “setup” involves quantifying the chosen combination of system variables.
  - b How reliable is the full scale setup prediction and what may influence prediction accuracy – State what additional aspects outside the model scope may influence the full scale setup prediction and give a qualitative impact. These aspects could include differences in control variables such as nozzle type or valve mechanism.

## 2 Theoretical Understanding

### 2.1 Gravity Valve Theory

In this section the theoretical understanding behind the gravity valve concept will be explored. Firstly schematic images are set up to help explain the system. Figure 2 shows the forces acting upon the system and system parameters. The two forces are the force due to the water jet stream and the force due to the valve's weight.

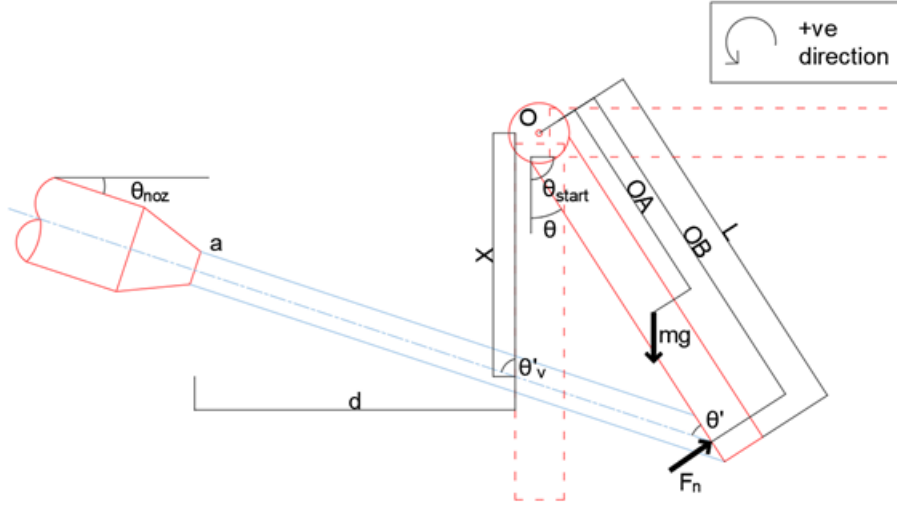


Figure 2: Schematic image showing all forces and variables influencing the gravity valve system.

All relevant system input parameters are:

- $\theta_{noz}$ : angle between nozzle and horizontal (rad)
- $\theta_{start}$ : valve's starting angle (rad)
- $L$ : valve length (m)
- $m$ : valve mass (kg)
- $OA$ : distance from pivot to valve centre of mass (m)
- $X$ : distance from pivot to jet impact when valve is vertical (m)
- $d$ : horizontal distance from nozzle to vertical valve (m)
- $a$ : jet stream area ( $m^2$ )
- $v_{noz}$ : jet velocity at nozzle exit (m/s)
- $\rho$ : density of water ( $kg/m^3$ )
- $g$ : acceleration due to gravity ( $m/s^2$ )

Subsequent dependent variables are:

- $\theta$ : angle of the valve with respect to the vertical axis (rad)
- $\theta'$ : angle made between the jet and valve (rad)
- $\theta'_v$ : angle between jet and valve when valve is vertical (rad)
- $\theta_{b+}$ : angle when valve loses contact with the jet in the positive theta domain (rad)
- $\theta_{b-}$ : angle when valve loses contact with the jet in the negative theta domain (rad)
- $F_n$ : force due to jet normal to the valve (N)
- $mg$ : force due to the valve's weight (N)
- $OB$ : distance from pivot to where  $F_n$  acts on the valve (m)

The research aims to use theory to model swing cycles over time and to understand to what extent input variables influence swing cycle behaviour. A complete swing cycle is defined as the valve swinging from and returning to its maximum angle. Throughout this complete cycle the valve experiences force due to its own weight when not in contact with the jet and force due to jet impulse

and own weight when in contact with the jet. The two important pulsing stream performance indicators are:

- Cycle time: Time taken for a complete jet open and jet closed period. This is equivalent to the valve swinging from and back to its initial position. Deltares desire a cycle time in the range of 1 to 6 seconds to mimic intermittent wave erosion.
- Jet open : close ratio: Ratio of time in which the jet stream is not being blocked compared to time in which the jet stream is being blocked. Deltares desire a high open : close ratio between 4 to 20. Jet close time should be limited to increase grass cover erosion over time, this reduces fire hose method experiment time and therefore cost.

Swing cycles will be modelled by calculating angular acceleration ( $\alpha$ ), angular velocity ( $\omega$ ) and valve angle ( $\theta$ ) over time ( $t$ ). Equations for  $\alpha$ ,  $\omega$  and  $t$  differ throughout a complete swing cycle due to different acting forces and changing trigonometric relations. Three phases are defined defined within a singular swing cycle where within each phase equations for  $\alpha$ ,  $\omega$  and  $t$  are constant. Figure 3 shows the three phases and six steps in each swing cycle, theta boundary angles separating each phase are also shown ( $\theta_{b+}$ ,  $\theta_{b-}$  and  $\frac{\pi}{2}$ ). The negative and positive boundaries where the valve enters or leaves the jet stream are indicated as well. The theta zero angle is defined as when the valve is vertical. Subsequently valve angles in phase 1 and 2 are positive and valve angles in phase 3 are negative. The valve's starting angle ( $\theta_{start}$ ) is chosen to be anywhere within phase 1, ranging between angles  $\theta_{b+}$  and  $\frac{\pi}{2}$ . Other starting angles are not considered because it takes time for the jet stream's characteristics to stabilise, therefore a valve angle which starts within the jet stream would not be practical. An overview of the direction of motion, forces acting and theta boundaries in each phase and step is shown in Table 1. Regarding direction of motion, anti clockwise swinging is defined as positive (+ve) and clockwise swinging is defined as negative (-ve).

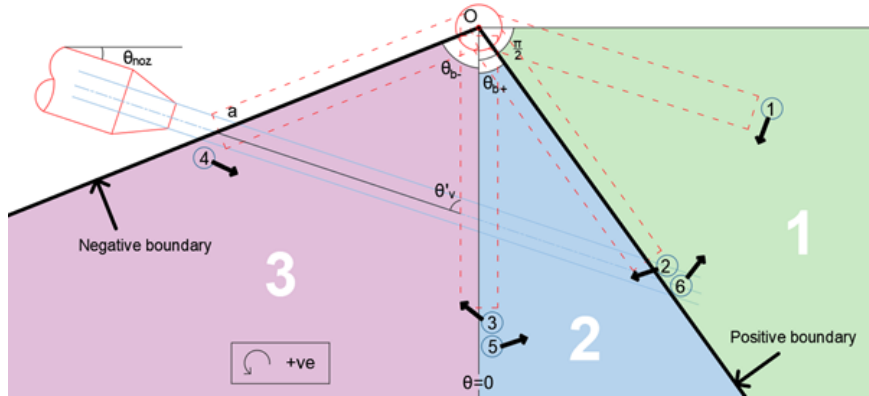


Figure 3: Demarcation of the gravity valve's swing cycle into three phases and six steps.

Table 1: Overview of the three defined gravity valve swinging phases and their subsequent steps.

Phase	Boundaries	Steps	Direction	Forces
1	$\theta_{b+} - \frac{\pi}{2}$	1-2	-ve	$mg$
		6-1	+ve	
2	$0 - \theta_{b+}$	2-3	-ve	$F_n mg$
		5-6	+ve	
3	$\theta_{b-} - 0$	3-4	-ve	$F_n mg$
		4-5	+ve	

To represent the gravity valve system a number of idealizations and assumptions have been made, they are:

- Ignore losses due to joint friction, air resistance and weather conditions (e.g. wind or rain).
- Assume jet velocity at nozzle is equal to jet velocity at valve impact.
- Assume the water jet acts as a straight beam of no area.
- Assume the water jet is an incompressible inviscid flow.

Firstly the dependent variables,  $\theta'_v$ ,  $\theta'$  and  $OB$  shown in Figure 2 are derived using trigonometry. Next trigonometric relations are used to derive negative and positive boundary angles shown in Figure 3. The negative boundary angle ( $\theta_{b-}$ ) is the angle in which the valve leaves the water stream when swinging in the negative direction, the valve swings through the water jet completely until it is no longer in contact with the jet or touches the nozzle. This creates a nonuniform pulsing pattern, thus if this negative boundary is exceeded the system is considered to fail. The positive boundary angle ( $\theta_{b+}$ ) is the angle between phase 1 and 2 in which the valve enters or leaves the water stream. Next, equations for torque due to the jet force ( $\tau_{Fn}$ ) and torque due to the valve weight ( $\tau_{mg}$ ) with respect to theta are derived. Force inflicted on the valve by the jet stream ( $F_n$ ) is determined using the impulse momentum principle where the impulse applied to the valve is directly related to the change in the jet stream's momentum. All calculations and derivations above are shown in Appendix A.

Next to determine the valves angle over time the angular version of Newton's second law is used as shown in Equation (1), where  $\sum \tau_o$  is the summation of torque from pivot point  $o$ ,  $I_o$  is the valve's moment of inertia from pivot point  $o$  and  $\alpha$  is the angular acceleration.

$$\sum \tau_o = I_o \alpha \quad (1)$$

From this relation equations for angular acceleration ( $\alpha$ ), angular velocity ( $\omega$ ) and time ( $t$ ) with respect to the valve's angle ( $\theta$ ) can be derived, final relations are shown in Equations (2), (3) and (4) respectively. Derivations of the equations are shown in Appendix A.

$$\alpha = \frac{\sum \tau_o}{I_o} \quad (2)$$

$$\omega d\omega = \alpha d\theta \quad (3)$$

$$dt = \frac{1}{\omega} d\theta \quad (4)$$

Equations for  $\alpha$ ,  $\omega$  and  $t$  with respect to  $\theta$  are derived for phases 1, 2 and 3 in sections A.1, A.2 and A.3 respectively. From these equations the valves movement over time can be analytically modeled as explained in Section 3.1 from which system cycle time and jet open : close ratio can be inferred.

Moment of inertia ( $I_o$ ) of the valve can be determined based on the valve's centre of mass,  $OA$ . Calculations and assumptions used to determine the valve's  $I_o$  value can be found in Appendix B.

## 2.2 Waterwheel Theory

In this section theoretical understanding of the waterwheel concept will be explored with the goal of predict waterwheel jet open : close ratios and cycle times and to explore how various input parameters effect them. This is achieved using two different methods. Method 1 uses the rough assumption that the waterwheel rotates at the same velocity as the jet stream. Method 2 considers forces acting on the system by using Newton's second law to derive equations for angular acceleration, angular

velocity and time with respect to the rotational angle, theta. In this report only two, three and four bladed waterwheels will be considered. Wheels with more blades are assumed to be unnecessary and will always result in undesirably small jet open : close ratios and cycle times. It should be noted that the waterwheel cycle time is taken as the time for one complete revolution. This is different to that of the gravity valve, for example during a two bladed waterwheel's complete revolution there are two complete pulse cycles (close-open-close-open) therefore to compare waterwheel cycle time to gravity valve cycle time you must divide waterwheel cycle time by the number of blades,  $n$ . The schematised version of the waterwheel system is shown in Figure 4, all input parameters and dependent variables are shown and explained below.

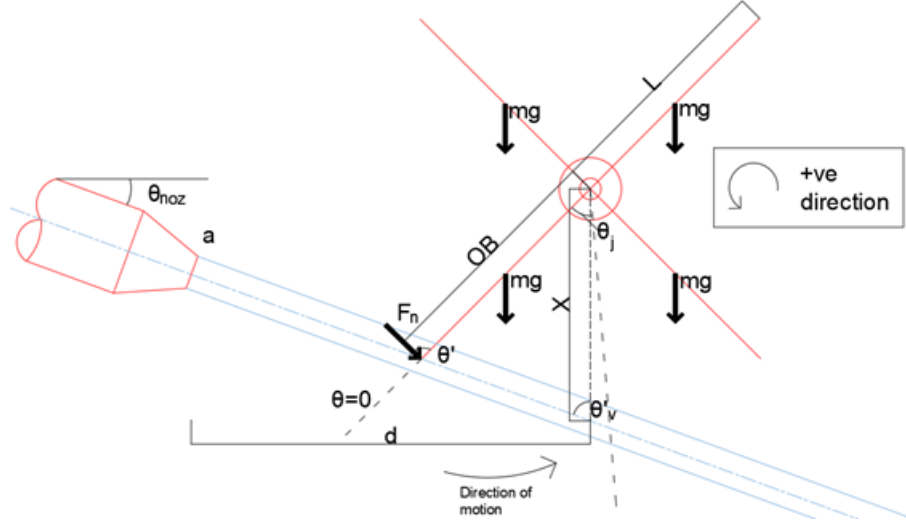


Figure 4: Schematic image showing all forces and variables influencing the waterwheel system.

All relevant system input parameters are:

- $\theta_{noz}$ : angle between nozzle and horizontal (rad)
- $n$ : number of blades (-)
- $L$ : blade length (m)
- $m$ : blade mass (kg)
- $OA$ : distance from pivot to blade centre of mass (m)
- $X$ : distance from pivot to jet impact when blade is vertical (m)
- $d$ : horizontal distance from nozzle to vertical blade (m)
- $a$ : jet stream area (m<sup>2</sup>)
- $v_{noz}$ : jet velocity at nozzle exit (m/s)
- $\rho$ : density of water (kg/m<sup>3</sup>)
- $g$ : acceleration due to gravity (m/s<sup>2</sup>)

Subsequent dependent variables are:

- $\theta$ : angle of the wheel's current revolution with respect to starting position 0 (rad)
- $\theta'$ : subsequent angle between jet and blade (rad)
- $\theta'_v$ : angle between jet and blade when valve is vertical (rad)
- $\theta_j$ : rotational angle during which the jet is blocked by a waterwheel blade (rad)
- $F_n$ : force due to jet normal to the blade (N)
- $mg$ : force due to the blades weight (N)
- $OB$  distance from pivot to where  $F_n$  acts on the valve (m)

Firstly the dependent variables used by both method 1 and 2 are derived.  $\theta'_v$  is derived, from which the boundary angle  $\theta_j$  can be derived. As shown in Figure 4,  $\theta_j$  is the rotational angle from  $\theta = 0$  during which the waterwheel blade is in contact with the jet stream. Waterwheel motion is chosen to start at  $\theta = 0$  which is when the first blade just touches the jet stream. The final derived equation

for  $\theta_j$  is shown in Equation (5). From  $\theta_j$ , the equation for  $\theta'$  can be derived. All derivations can be found in Appendix C. It should be noted that  $X$  can be slightly greater than the blade length ( $L$ ) and the jet stream can still make contact with the waterwheel blades. This is because  $X$  is defined as the vertical distance, instead of perpendicular distance from the waterwheel pivot to the jet stream.

$$\theta_j = \pi - 2\sin^{-1}\left(\frac{X\sin(\theta'_v)}{L}\right) \quad (5)$$

### 2.2.1 Method 1: Jet Velocity Assumption

Next, method 1, the jet velocity assumption method is presented. The method involves converting the jet stream's vector velocity into wheel's angular velocity. Conversion of vector velocity to angular velocity depends on the distance from the jet impact (point where vector velocity acts) to the wheel pivot ( $OB$ ). As the wheel rotates,  $OB$  and thus the angular velocity change due to geometry. The wheel's angular velocity is assumed to be constant and equal to the average angular velocity during a cycle. The method employs the following idealizations and assumptions:

- Assume the waterwheel spins at constant angular velocity,  $\omega$  equivalent to that of the constant vector water jet velocity.
- Assume jet velocity at nozzle is equal to jet velocity at blade impact.
- Assume the water jet acts as a straight beam of no area.
- Consider the waterwheel blades to have zero thickness.

Firstly vector jet stream velocity perpendicular to the blade ( $v$ ) is converted to angular velocity ( $\omega$ ) using the relationship  $\omega = \frac{v}{OB}$ . As mentioned before, angular velocity changes as the wheel rotates because both  $v$  and  $OB$  values are dependent on the wheel's rotational angle ( $\theta$ ). The average value of  $\omega$  throughout the angle in which the blade is in contact with the jet ( $\theta_j$ ) is determined using integration, the final equation for average angular velocity of the wheel is shown in Equation (6). From the average constant angular velocity cycle time can be determined. As the waterwheel is assumed to spin at a constant velocity, the jet open:close ratio can be determined using the angle during which the jet is blocked ( $\theta_j$ ) and the angle during which the jet is open. All detailed calculations and derivations of method 1 cycle time and open:close ratio can be found in Appendix C.1.

$$\omega_{avg} = \frac{1}{\theta_j} \left( \int_0^{\theta_j} \frac{\sin(\theta_{j1} - \theta + \theta'_v)v_{noz}}{\frac{X\sin(\theta'_v)}{\sin(\theta_{j1} - \theta + \theta'_v)}} d\theta \right) \quad (6)$$

### 2.2.2 Method 2: Force Considerations

Lastly, method 2, the force consideration method is calculated. Like the gravity valve theory, the method uses the angular version of Newton's second law shown in Equation (1) to derive relations for angular acceleration ( $\alpha$ ), angular velocity ( $\omega$ ) and time ( $t$ ) as shown in Equations (2), (3) and (4) respectively. From the relations the waterwheel's angle ( $\theta$ ) over time can be determined from which system cycle time and jet open : close ratio can be inferred. The method employs the following idealizations and assumptions:

- Assume the wheel's angular velocity is less when not in contact with the jet, this reduced velocity compensates for energy losses and helps the wheel reach an equilibrium of constant angular velocity.
- Assume jet velocity at nozzle is equal to jet velocity at valve impact.
- Assume the water jet acts as a straight beam of no area.
- Consider the waterwheel blades to have zero thickness.
- Assume the water jet is an incompressible inviscid flow.

Firstly the equation for torque due to the jet force ( $\tau_{Fn}$ ) is derived. There is no torque due to blade weight as the torque equates to zero at any random waterwheel position as blades act both in positive and negative directions at the same magnitude. This holds for the two, three and four bladed waterwheels studied. Next, the equations for  $\alpha$ ,  $\omega$  and  $t$  with respect to  $\theta$  are determined. Using the equations, waterwheel movement over time can be analytically modelled. This process is presented in Section 3.2. Currently due to the use of Newtonian mechanics, no energy losses are considered, this results in the waterwheel infinitely gaining velocity each time it comes into contact with the jet. Therefore it is assumed that the waterwheel velocity decreases when not in contact with the jet. This helps account for energy losses and will allow a constant angular velocity to be reached as observed empirically. The magnitude of velocity decrease is calibrated based on experimental results in Section 5.2.2.

The waterwheel's moment of inertia is determined by multiplying  $I_o$  of each identical blade by the number of blades in each wheel ( $n$ ). The moment of inertia of each blade is determined based on  $OA$  using equations derived in Appendix B.

### 3 Analytical Model Development

#### 3.1 Gravity Valve Model Development

In this section the gravity valve analytical model is explained. The model's purpose is to assess whether the non-powered gravity valve concept is feasible and to provide insight into how input parameters influence its performance. The model aims to predict valve angle ( $\theta$ ), angular acceleration ( $\alpha$ ) and angular velocity ( $\omega$ ) over time ( $t$ ). From this data cycle time and jet open:close ratios can be determined which are used as the main system performance indicators. Each swing cycle contains three phases and six steps as shown in Figure 5. Each phase uses different equations to determine  $\alpha$ ,  $\omega$  and  $t$  as explained in Section 2.1. An overview of the equations applied in each phase is shown in Table 2.

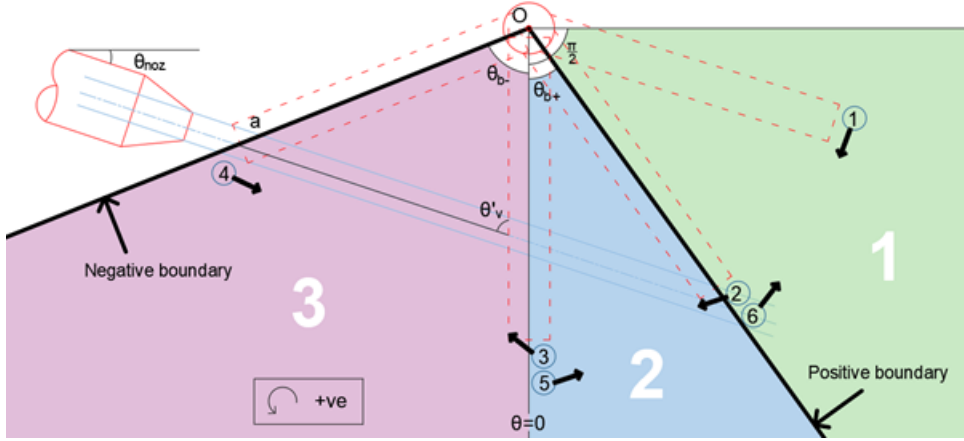


Figure 5: Demarcation of the gravity valve's swing cycle into three phases and six steps.

Table 2: Overview of all equations used by the gravity valve model for each phase and step.

Phase	Steps	Equations
1	1-2	$\alpha_1 = \frac{-mgOAsin(\theta)}{I_o}$
	5-1	$\omega_1 = \left( \frac{2(mgOAcos(\theta)) - mgOAcos(\theta_i)}{I_o} + \omega_i^2 \right)^{0.5}$ $t_1 = \int_{\theta_i}^{\theta} \frac{1}{\left( \frac{2(mgOAcos(\theta)) - mgOAcos(\theta_i)}{I_o} + \omega_i^2 \right)^{0.5}} d\theta + t_i$
2	2-3	$\alpha_2 = \frac{\rho av^2 X sin(\pi - \theta'_v) - mgOAsin(\theta)}{I_o}$
	5-6	$\omega_2 = \left( \frac{2((\rho av^2 X sin(\pi - \theta'_v)\theta + mgOAcos(\theta)) - (\rho av^2 X sin(\pi - \theta'_v)\theta_i + mgOAcos(\theta_i)))}{I_o} + \omega_i^2 \right)^{0.5}$ $t_2 = \int_{\theta_i}^{\theta} \frac{1}{\left( \frac{2((\rho av^2 X sin(\pi - \theta'_v)\theta + mgOAcos(\theta)) - (\rho av^2 X sin(\pi - \theta'_v)\theta_i + mgOAcos(\theta_i)))}{I_o} + \omega_i^2 \right)^{0.5}} d\theta + t_i$
3	3-4	$\alpha_3 = \frac{\rho av^2 X sin(\theta'_v) + mgOAsin(-\theta)}{I_o}$
	4-5	$\omega_3 = \left( \frac{2((\rho av^2 X sin(\theta'_v)\theta + mgOAcos(-\theta)) - (\rho av^2 X sin(\theta'_v)\theta_i + mgOAcos(-\theta_i)))}{I_o} + \omega_i^2 \right)^{0.5}$ $t_3 = \int_{\theta_i}^{\theta} \frac{1}{\left( \frac{2((\rho av^2 X sin(\theta'_v)\theta + mgOAcos(-\theta)) - (\rho av^2 X sin(\theta'_v)\theta_i + mgOAcos(-\theta_i)))}{I_o} + \omega_i^2 \right)^{0.5}} d\theta + t_i$

The model runs each swing cycle step sequentially using final angular velocity and angle output of the previous step as initial angular velocity and angle input for the next step. The model accommodates starting angles within phase 1, ranging between angles  $\theta_{b+}$  and  $\frac{\pi}{2}$  as shown in Figure 5. Other starting angles are not considered; it takes time for the jet streams characteristics to stabilise therefore a valve angle which starts within the jet stream would not be practical. Additionally

different starting angles provide no benefit to the functionality of the system.

Before calculating each step the theta boundaries must be known to determine which theta limit values to apply to  $\omega$  equations and  $t$  integrals. In the model  $\theta_i$  is defined as the initial theta boundary value and  $\theta_f$  is defined as the final theta boundary value for each swing section. The initial omega ( $\omega_i$ ) and time ( $t_i$ ) values must also be known to complete  $\omega$  equations and  $t$  integrals. Figure 6 shows  $\theta$ ,  $\omega$  and  $t$  values for each of the six swing steps. A swing section of for example 1-2, would have initial values as shown in box 1 and final theta values as shown in box 2.  $\omega$  and  $t$  values are often derived as the final value from the previous step. For example the initial  $\omega$  value at point two is the final  $\omega$  value at the end of step 1-2 ( $\omega_{f1-2}$ ). As shown in the blue box, the model determines if the valve swings into phase 3 (the negative theta section) by determining whether a solution exists for  $\omega_2(\theta)$  equalling zero within phase two. If  $\omega$  is zero it is assumed the valve instantaneously comes to rest and begins swinging back in the opposite direction thus not reaching phase 3. If there is no solution it is assumed the valve swings into the negative theta domain and comes to rest there. As done in the red boxes, maximum theta swing angles can be found by solving  $\omega$  equations for when  $\omega$  equals zero as the valve is assumed to come to rest at maximum and minimum swing angles.

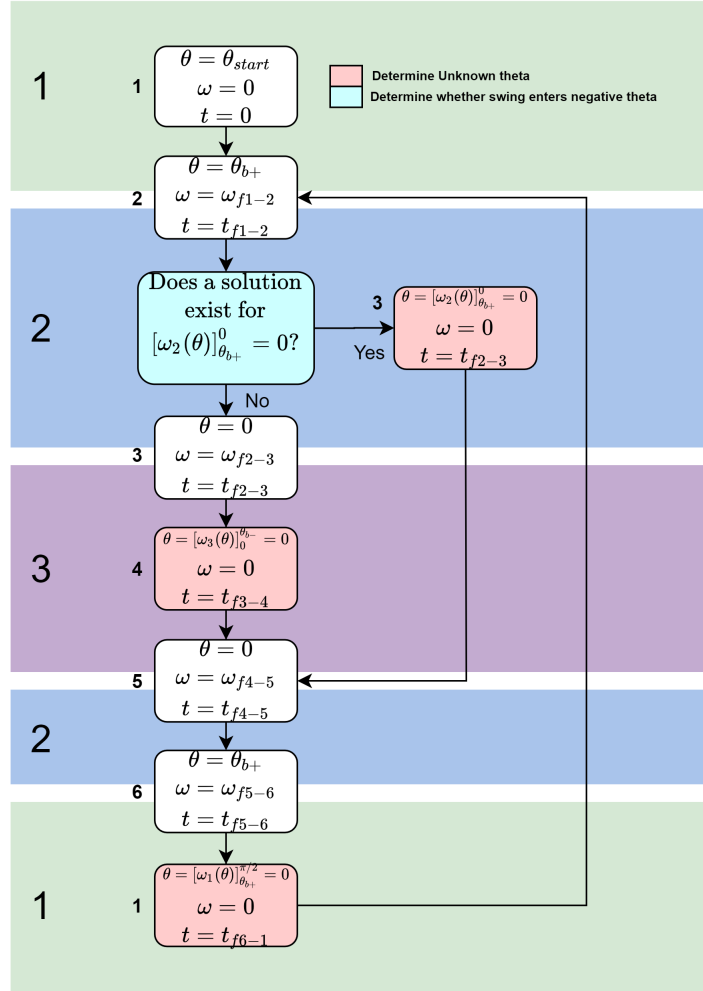


Figure 6: How initial theta, angular velocity and time values are found at each of the six gravity valve swing cycle points.

Once initial values are determined, the equations shown in Table 2 can be applied. When the valve is swinging in the negative direction (steps 1-2, 2-3 and 3-4) equations for  $\omega$  and  $t$  are negative as theta integral limits are applied the other way round. A few exitflag scenarios have been devised to determine whether the system performs as desired. These exitflag scenarios are;

- Exitflag 1: The valve swing exceeds the negative theta boundary ( $\theta_{b-}$ ) resulting in an unde-

sirable non-uniform pulsing pattern.

- Exitflag 2: Torque due to gravity is too great and the valve reaches an equilibrium as the valve comes to rest in phase two resulting in a permanently blocked stream.
- Exitflag 3: The systems valve open : close ratios are insufficient. Deltares prefer a system with an open :close ratio greater than four. Larger periods of open flow allows for quicker dike erosion resistance tests ultimately saving money, time and resources.

The flow chart shown in Figure 7 explains how swing steps, initial values and exitflags interact and function within the MATLAB model. The complete MATLAB model code is shown in Appendix D.

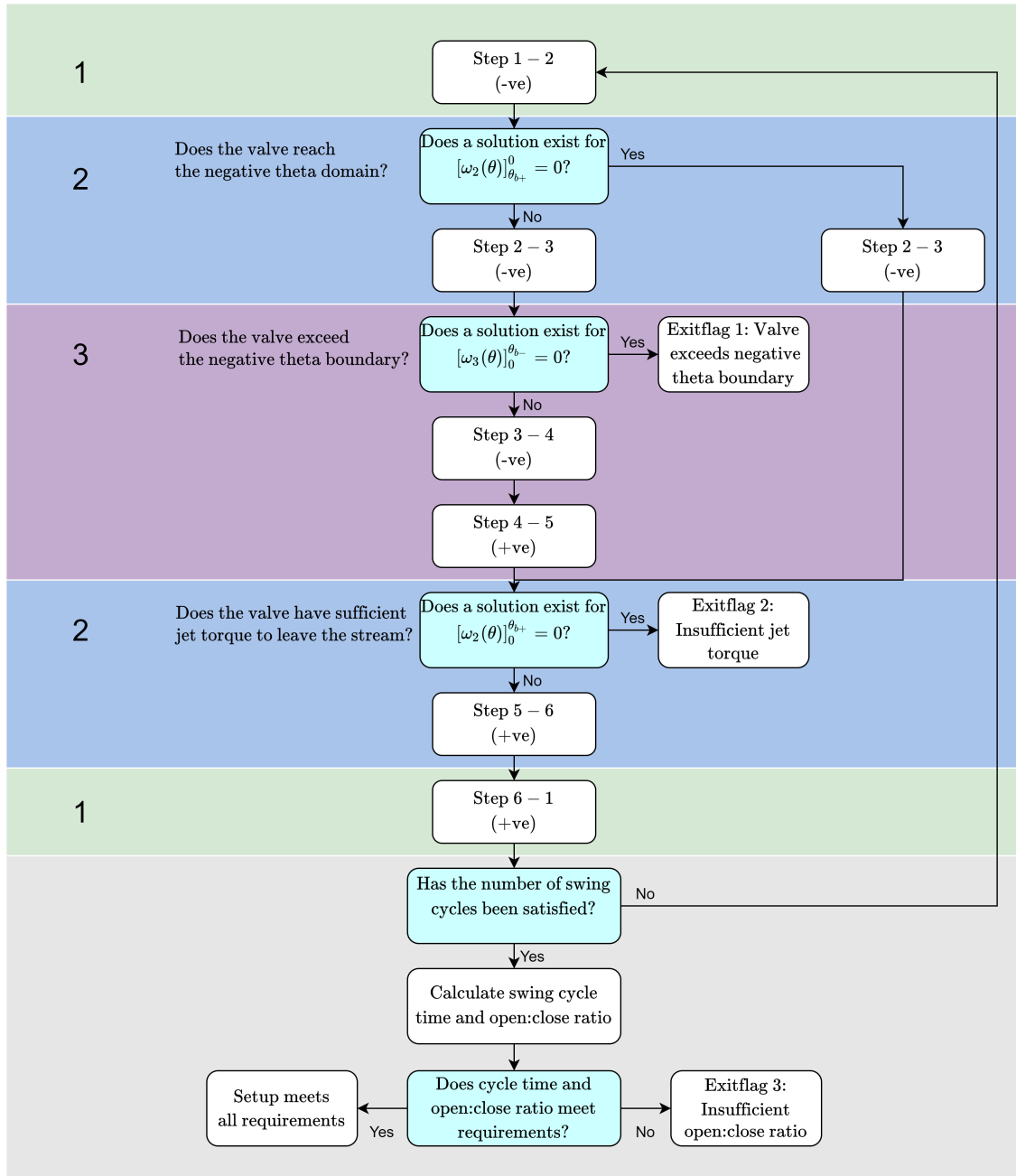


Figure 7: Flow chart showing how gravity valve MATLAB model functions.

### 3.2 Waterwheel Model Development

In this section the waterwheel analytical model is explained for both method 1 and method 2. The waterwheel model's purpose is to predict how varying input parameters effect the waterwheel cycle time and jet open:close ratio performance. During waterwheel system modelling no exitflags were considered, meaning it is assumed that the waterwheel always creates a pulsing water stream. In reality there are two instances when the system fails to create a pulsing water stream. The first is when the wheel cannot even be moved because torque due to the jet force is so low compared to the resisting force of the wheel's mass and subsequent moment of inertia. The second instance is when a very low  $X$  value is chosen, so the jet impacts the waterwheel blade too close to the pivot, thus the jet stream is always blocked and a pulsing stream is not achieved.

Modelling for method 1, the jet velocity assumption method, is straightforward and simply involves applying Equations derived in Appendix C.1. Equation (58) is integrated within MATLAB to get average angular velocity from which the cycle time can be determined using Equation (59). The jet open:close ratio can then be found by determining  $\theta_j$  using Equation 52 which can then be used to find jet open:close ratio by applying Equation (60).

Modelling method 2 requires more complex modelling steps and structure. Firstly the waterwheels moment of inertia is determined by multiplying the moment of inertia of each blade by the number of blades. The moment of inertia of each blade is determined based on the blades chosen centre of mass,  $OA$  as shown in Appendix B. Next, the dependent variables  $\theta'_v$  and rotational angle in which the wheel is in contact with the jet,  $\theta_j$  are determined. Next anonymous functions derived in Appendix C.2 for waterwheel angular acceleration, angular velocity and time with respect to theta are defined in the MATLAB model. These functions are shown in Table 3.

Table 3: Three equations used to determine waterwheel motion when in contact with the jet stream.

Value	Derived Equation
Angular acceleration ( $\alpha$ )	$\alpha = \frac{\rho av^2 X \sin(\theta'_v)}{I_o}$
Angular velocity ( $\omega$ )	$\omega = \left( \frac{2((\rho av^2 X \sin(\theta'_v)\theta) - (\rho av^2 X \sin(\theta'_v)\theta_i))}{I_o} + \omega_i^2 \right)^{0.5}$
Time ( $t$ )	$t = \int_{\theta_i}^{\theta} \frac{1}{\left( \frac{2((\rho av^2 X \sin(\theta'_v)\theta) - (\rho av^2 X \sin(\theta'_v)\theta_i))}{I_o} + \omega_i^2 \right)^{0.5}} d\theta + t_i$

Once initial values and equations are defined the modelling of the waterwheel's movement can begin. The process followed by the MATLAB model is shown in Figure 8. Firstly, the period when the waterwheel is in contact with the jet is modelled, this is modelled using the equations shown in Table 3. Once modelled the time taken for the movement is recorded, this is the time in which the jet is closed,  $t_{jc}$ . Next the period when the waterwheel is not in contact with the jet is modelled. During this period the waterwheel is assumed to rotate at a lower angular velocity. This is necessary otherwise the waterwheel would continue to gain velocity everytime the blade comes into contact with the jet, this is because theoretical understanding uses Newton's second law which does not consider energy losses. By applying this lower velocity during no jet contact the model eventually predicts the wheel to converge at a constant velocity as observed in reality. This lower angular velocity is equal to a constant, the no jet deceleration constant ( $njdC$ ) multiplied by  $\omega_i$ .  $njdC$  is calibrated to fit empirical data as shown in Section 5.2.2. Once modelled the time taken for the no-jet movement and thus the time in which the jet is open is recorded ( $t_{jo}$ ). This process is repeated until all waterwheel blades are modelled, for example if the waterwheel had three blades this process would be repeated twice more. Once an entire revolution is modelled ( $\theta = 2\pi$ ) the cycle time and jet open:close ratio can be determined for that revolution based on jet open and

close times. This process is repeated until the desired number of revolutions are modelled and the waterwheel cycle time has converged to a constant value.

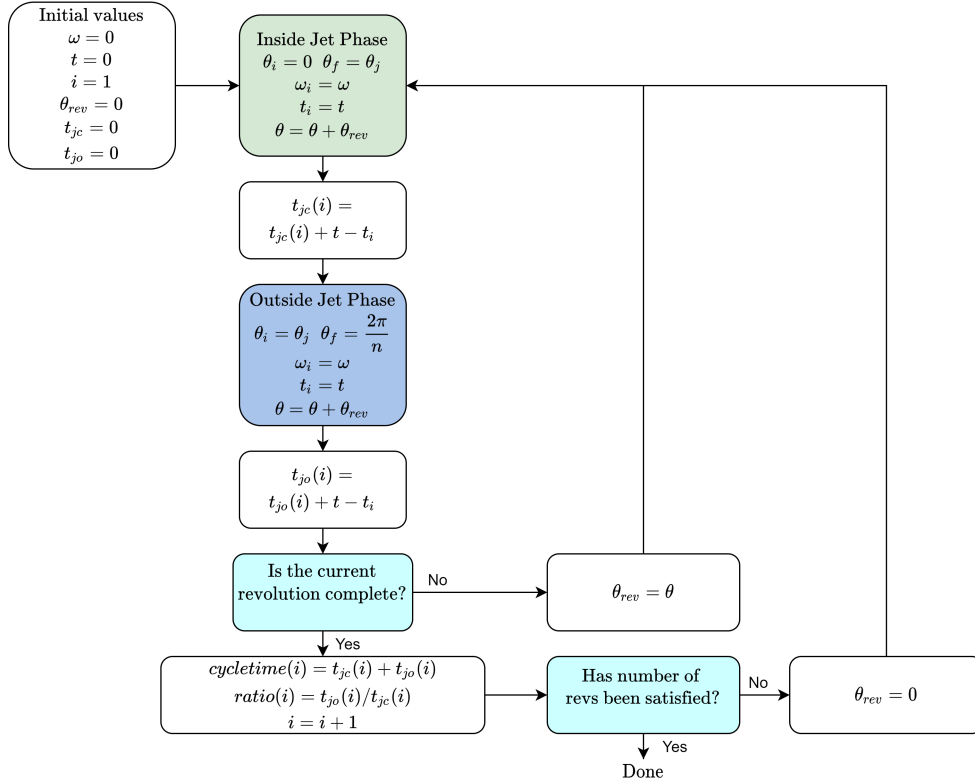


Figure 8: Flow chart showing how waterwheel MATLAB model functions.

The complete MATLAB model code for both methods is shown in Appendix E.

## 4 Experimental Procedure

### 4.1 Gravity Valve Experimental Set-up

In this section the gravity valve's experimental set-up and procedure is explained. The purpose of the physical experimentation is to observe whether a gravity valve set-up actually creates a lasting pulsing water stream and to collect empirical data to compare to model results. The experiment was conducted in a back garden with basic tools therefore parameters and results are measured with limited accuracy. An impression of the physical experiment is shown in Figure 9 which consists of the following main components:

- Garden hose
- Jet nozzle
- Hose frame
- Metal valve
- Valve frame
- Ten litre bucket
- Flow measure device
- Camera



Figure 9: Impression of the physical experimental setup used to test the gravity driven pivot valve theory.

Firstly the jet stream characteristics are measured. The jet stream area ( $a$ ) is simply measured with a ruler to be circular with a diameter of 5 mm to the nearest mm. This equates to a jet stream area of  $0.00007854 \text{ m}^2$ . The jet velocity at the nozzle ( $v_{noz}$ ) is derived from the flow rate ( $Q$ ) and the jet area ( $v = Q/a$ ). The flow rate is measured using both a flow measure device and by timing how long it takes to fill a ten litre bucket. Both methods read a flow rate of 12 litres per minute to the nearest litre. This equates to a nozzle flow velocity of 2.55 m/s.

Next the nozzle and valve are set up. The valve's length ( $L$ ) is measured to the nearest mm and the mass is weighed to the nearest gram. The nozzle is placed against the wooden board frame and clamped at 20 degrees. The valve is slotted into its frame. A metal rod is glued to the top edge of the valve and then slotted between two metal eye bolts on the frame. This joint is kept lubricated with WD-40 to reduce friction. The horizontal distance from the nozzle to the vertical valve ( $d$ ) is

set using a ruler to 25 cm to the nearest cm. Four different valves are tested, each with different lengths and masses. Every valve except valve 1 is tested at three different values of  $X$ , valve 1 is tested at two  $X$  values as it is shorter ( $L=0.1$  m). The  $X$  value's are adjusted by moving the clamped nozzle up and down. Three different jet nozzle velocities, namely 2.55, 2.088 and 1.769 m/s are also tested to try and gain empirical insight into jet : weight torque ratio influence.  $\theta_{start}$  is kept at  $\frac{\pi}{2}$  however human error may cause some start angle variation. An overview of all 33 conducted tests is shown in Table 4.

Each test is recorded using a camera placed perpendicular to the valve. The footage is then re-watched in slow motion from which  $X$  can be precisely measured. Only the angle of maximum and minimum swings and their subsequent times are measured. The process is labour intensive and involves identifying maximum and minimum swing angles in the footage, noting their times, taking a screenshot of the video frame and measuring the swing angles from the image in AUTOCAD.

Table 4: Overview of the 33 physical gravity valve tests conducted using four different valve types.

Test	$X$ (m)	$v_{noz}$ (m/s)	$L$ (m)	$m$ (kg)	$OA$ (m)
1.1	0.063	2.55	0.1	0.128	0.05
		2.088			
		1.769			
1.2	0.071	2.55	0.15	0.224	0.075
		2.088			
		1.769			
2.1	0.072	2.55	0.15	0.224	0.075
		2.088			
		1.769			
2.2	0.078	2.55	0.15	0.224	0.075
		2.088			
		1.769			
2.3	0.127	2.55	0.15	0.224	0.075
		2.088			
		1.769			
3.1	0.081	2.55	0.2	0.164	0.1
		2.088			
		1.769			
3.2	0.131	2.55	0.2	0.164	0.1
		2.088			
		1.769			
3.3	0.153	2.55	0.2	0.164	0.1
		2.088			
		1.769			
4.1	0.061	2.55	0.15	0.175	0.075
		2.088			
		1.769			
4.2	0.076	2.55	0.15	0.175	0.075
		2.088			
		1.769			
4.3	0.12	2.55	0.15	0.175	0.075
		2.088			
		1.769			

## 4.2 Waterwheel Experimental Set-up

In this section the waterwheel's experimental set-up and procedure is explained. The purpose of the waterwheel physical experimentation is to observe whether a lasting pulsing water stream is created and to collect experimental cycle time data to compare to model results. The experiment was conducted in a back garden with basic tools therefore parameters and results are measured with limited accuracy. An impression of the physical experiment is shown in Figure 9 which consists of the following main components:

- Garden hose
- Jet nozzle
- Hose frame
- 20 degree mould
- Wooden waterwheel (two, three and four blades)
- Waterwheel frame
- Ten litre bucket
- Flow measure device
- Camera



Figure 10: Impression of the physical experimental setup used to test the waterwheel theory.

The experiment uses the same jet stream characteristics as the gravity valve experiment. Namely a jet stream with an area of  $0.00007854 \text{ m}^2$  which is tested at different velocities of 2.55, 2.088 and 1.769 m/s. The waterwheels used are made of plywood. A tight hole is drilled through the centre of each wheel and a metal rod is inserted as the axis. Each waterwheel has a blade length of 0.15 m

however both length and moments of inertia can be altered by taping longer blades or metal weights to the waterwheels. The waterwheels are slotted into their frame and are held by two eyehooks, WD-40 is used to reduce friction. The nozzle is setup and clamped to its desired  $X$  height. The nozzle is kept at 20 degrees using a 20 degree measuring mould. The horizontal distance from the nozzle to the vertical valve ( $d$ ) is set using a ruler to 25 cm to the nearest cm.

An overview of the 21 waterwheel tests conducted is shown in Table 5. Three different variations of  $X$ ,  $I_o$ ,  $L$  and  $v_{noz}$  are tested using the two bladed wheel whilst all other variables are kept constant to help identify trends and how input parameters effect waterwheel cycle time. Each test is performed three times and average values are taken to reduce error. Three and four bladed wheels are also tested with three different  $v_{noz}$  values. One three bladed wheel test also involves testing the feasibility of a braking system to increase cycle time. The braking system is very primitive and simply consists of a fixed stick applying friction to the three bladed waterwheel as shown in Appendix F, Figure 32. The braking system is tested on the three bladed wheel as it was easier to apply friction to the wooden circular plates used explicitly in the three bladed wheel construction. After performing the experiments the test footage is re-watched in  $0.01\times$  slow motion from which  $X$  values can be precisely measured. The revolution number and subsequent time is measured. From this waterwheel cycle time can be determined. The process is labour intensive and not very accurate because the waterwheel spins so quickly that the camera footage is not fast enough to keep up, each revolution only contains 4-5 frames therefore the time taken for a complete revolution must be somewhat estimated between frames. This issue is especially problematic for the three and four bladed waterwheels wheres it is difficult to differentiate between blades throughout frames.

Table 5: Overview of the 21 physical waterwheel tests conducted.

Test	$n$ (-)	$X$ (m)	$I_o$ (kg m <sup>2</sup> )	$L$ (m)	$v_{noz}$ (m/s)
1.1		0.062	0.000728	0.15	2.55
		0.122			
		0.159			
1.2	2	0.097	0.000728	0.15	2.55
			0.001726		
			0.001994		
1.3		0.14	0.000728	0.15	2.55
		0.178		0.20	
		0.254		0.25	
1.4		0.097	0.000728	0.15	2.55
					2.088
					1.769
2.1	3	0.128	0.001091	0.15	2.55
					2.088
					1.769
2.2	3 brake	0.128	0.001091	0.15	2.55
					2.088
					1.769
3.1	4	0.138	0.001125	0.15	2.55
					2.088
					1.769

## 5 Results

### 5.1 Gravity Valve Results

#### 5.1.1 Gravity Valve Model Results

In this section gravity valve model results are shown. The main model output is theta over time, from which cycle time and valve open : close ratio can be derived. The main insight is that the valve is modelled to always return to its starting angle.

In terms of order of magnitude, model results for swing cycle times seem plausible. They are comparable to pendulum theory time periods. For example using Equation (7), for pendulum time period ( $T_0$ ), a pendulum of length ( $l$ ) 0.15 m has a time period of 0.78 seconds. The model determines a 0.15 m long valve to have a similar time period of 0.5-0.75 s depending on the realistically chosen input parameters.

$$T_0 = 2\pi\sqrt{\frac{l}{g}} \quad (7)$$

Using theoretical background knowledge, four non dimensional system setup parameters are chosen to be tested to see their influence on model output. Using non dimensional values to test input-output relationships helps create wider result applicability useful for system upscaling. The non dimensional parameters also group a number of input parameters together helping to simplify the system and save time. The four parameters tested are:

1. Jet : weight torque ratio.

- Theoretically the most significant parameter as torque exerted on the valve by the jet stream and the valves own weight are fundamental in determining the magnitude of the valve’s angular acceleration from which angular velocity and time are derived. This indicator includes parameters  $\rho, a, v, X, L, m, g, OA, \theta_{noz}$  and  $\theta$ .

2. The ratio between the valve length and  $X$  ( $L : X$  ratio).

- The position of  $X$ , distance from pivot to jet impact when the valve is vertical is influential in determining positive and negative theta boundaries and determining torque due to the jet stream.

3. The ratio between the valve length and the valve centre of mass from the pivot ( $L : OA$  ratio).

- The position of  $OA$ , the valves centre of mass from the pivot is influential in determining the moment of inertia and the magnitude of the torque due to the valve weight.

4. The valve’s starting angle,  $\theta_{start}$ .

- The valve starting angle effects the angle boundaries of phase 1.

Using the model, the influence of non dimensional parameters on the pulsing water streams performance. Cycle time (the time taken for a complete jet open and jet closed period) and jet open : close ratio (the ratio of time the jet is open compared to closed) are calculated for different non dimensional parameter values. When testing a non dimensional parameter’s influence on pulsing stream performance, all other parameters and thus non dimensional parameters are kept at constant ”baseline” values. For example when testing jet : weight torque ratio,  $L : X$ ,  $L : OA$ ,  $\theta_{start}$  and all other parameters are kept constant. The constant baseline parameters are chosen at both the small experimental set up scale as well as Deltares’ full scale set up. This is to determine whether non dimensional parameter relations can be upscaled. Baseline parameters used for tests on both scales are shown in Table 6. All baseline non dimensional parameters are also the same for two different

scale tests, for example both scales have the same jet : weight torque ratio, this is ensured by giving Deltares' full scale test a much heavier valve to counteract the greater jet stream torque. Model results for all four non dimensional parameters show that both the small scale and full scale values give the same results. This proves the effectiveness of the non dimensional parameters.

Table 6: Overview of the baseline parameters used for each gravity valve model test.

Parameter	Experiment set-up base-line values	Deltares full scale set-up baseline values
$L$ (m)	0.15	0.15
$m$ (kg)	0.2	38.38
$X$ (m)	0.075	0.075
$OA$ (m)	0.075	0.075
$v_{noz}$ (m/s)	2.55	7
$a$ (m <sup>2</sup> )	0.00007854	0.002
$d$ (m)	0.25	0.25
$\theta_{noz}$ (deg)	20	20
$\theta_{start}$ (rad)	$\frac{\pi}{2}$	$\frac{\pi}{2}$

Results for influence of the jet : weight torque ratio are shown in Figure 11. Valve mass,  $m$  is altered to control the ratio. The jet : weight torque ratio does appear to be the most influential of the non dimensional parameters, a ratio of less than 0.0645 results in the valve weight torque being too great and causes the system to fail as the valve swings all the way through the jet until it exceeds the negative boundary and leaves the jet stream. As the jet : weight torque ratio increases, cycle time decreases whilst valve open : close ratio increases. This is logical as the jet torque becomes more powerful than the valve weight torque and after a certain point it can instantly push the valve back open upon contact with the jet.

Results for influence of the  $L : X$  ratio are shown in Figure 12. The  $L : X$  ratio is changed by altering  $X$  values. Any ratio less than 1.19 results in the valve exceeding the negative boundary because contact time with the jet is too small to provide enough resistance to the valve's weight torque. It should be noted that this minimum ratio is also dependent on all three other non dimensional parameters. There is no upper limit for  $L : X$  ratio, as  $L : X$  ratio increases cycle time increases due to increasingly smaller jet torque due to the smaller  $X$  value. Open : close ratios decrease as  $L : X$  ratio increases as time in contact with the jet increases due to larger theta positive boundary angles.

Results for influence of the  $L : OA$  ratio are shown in Figure 13. The relationships are strikingly similar to that of the jet : weight torque ratio. This is because  $OA$  influences weight torque and moment of inertia just as valve mass ( $m$ ) does which was altered to control the jet : weight torque ratio. Any ratio less than 1.07 results in the valve exceeding the negative boundary as the torque due to the valve weight becomes too great. As the  $L : OA$  ratio increases (valves centre of mass moves closer to the pivot) cycle time decreases as torque due to valve weight decreases resulting in smaller angled and thus quicker swing cycles. The open : close ratio increases strongly as a very high  $L : OA$  ratio creates a very small torque due to valve weight, causing the much stronger jet torque to instantly push the valve out of the jet stream.

Results for influence of  $\theta_{start}$  are shown in Figure 14. Tested  $\theta_{start}$  values range from the positive boundary to  $\frac{\pi}{2}$ . Larger  $\theta_{start}$  values cause larger open : close ratios. This is logical as the valve returns to  $\theta_{start}$ , if  $\theta_{start}$  is larger the valve will spend more time outside of the jet stream. Larger  $\theta_{start}$  values also cause greater swing angles which increase cycle times although the magnitude of this effect is not too significant.

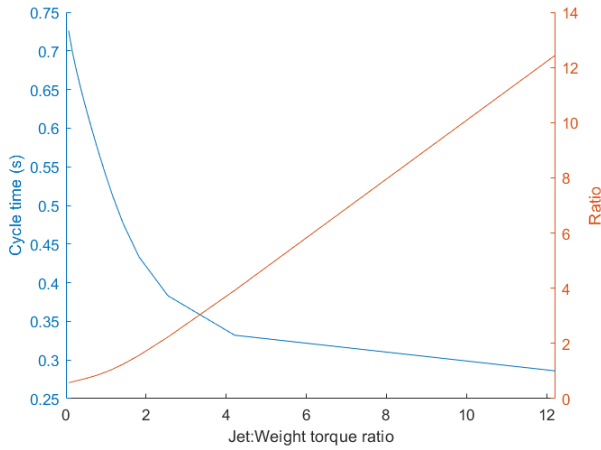


Figure 11: Effect of jet : weight torque ratio on gravity valve's cycle time and open : close ratio.

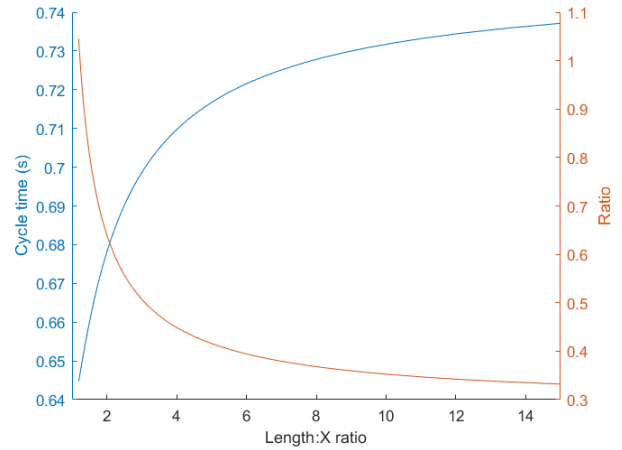


Figure 12: Effect of valve length : X ratio on gravity valve's cycle time and open : close ratio.

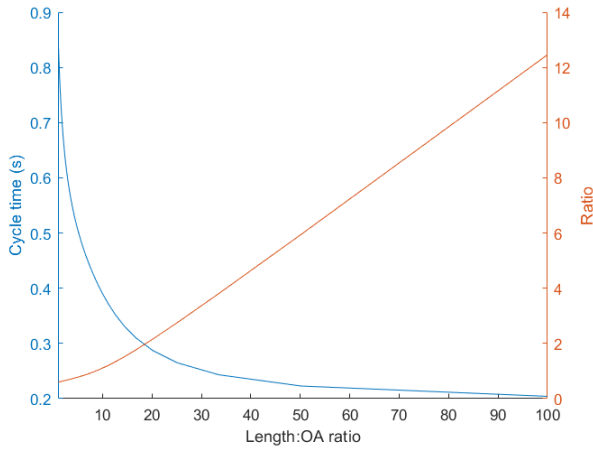


Figure 13: Effect of valve length : OA ratio on gravity valve's cycle time and open : close ratio.

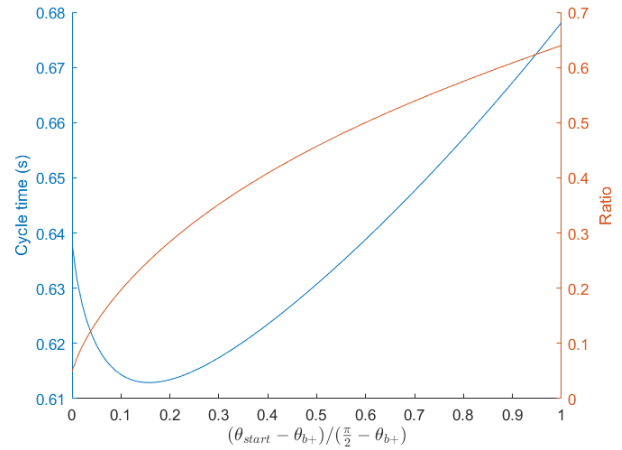


Figure 14: Effect of  $\theta_{start}$  on gravity valve's cycle time and open : close ratio.  $\theta_{start}$  ranges from the positive boundary (0) to  $\pi/2$  (1).

Based on model results, to achieve Deltares' desirable valve open : close ratios of 4 or more, high jet : weight and  $L : OA$  ratios would be required. A powerful jet would limit valve time in the jet and a valve centre of mass nearer the pivot would lower the torque due to valve weight also helping to limit valve time in the jet. However, increasing jet : weight torque and  $L : OA$  ratios decreases cycle time. For example a jet : weight torque and  $L : OA$  ratio that achieves a valve open : close ratio of four results in a cycle time of 0.35 seconds, which is well below Deltares' desired range of 1-6 seconds.

### 5.1.2 Gravity Valve Experiment Results

In this section gravity valve experimental results are shown and compared to modelling predictions. Experimental observations show that all tested system set ups experience dampening effects and after only 4-5 swing cycles the valve reaches a stationary situation that converges around the positive theta boundary and constantly blocks the stream. Only cycle time data is recorded, ratio data couldn't be accurately measured with the available equipment and time constraints.

Some of the 33 tests shown in Table 4 were analysed and compared against model predictions. Figure 15 shows the valves angle over time for test 1.1 from Table 4 where three different nozzle velocities were tested. The valve starts in the horizontal position,  $0.5 \pi$  rad. The model correctly predicts the trend that a greater jet velocity results in a shorter cycle time. However cycle time observations are not in line with model predictions, the model fails to account for the heavy dampening effects observed in the experiment. The model predicts longer cycle times due to the valve's deep swings into the jet stream reaching angles of nearly  $-0.4 \pi$  radians. However in reality cycle times are much shorter as the jet stream heavily resists the swinging motion. The model seems to either underestimate torque exerted due to the jet stream or over estimate torque due to the valves own weight.

Results for test 2 are shown in Figure 16 where three different  $X$  values are tested at  $v_{noz}$  values of 2.55 m/s on a 0.15 m long valve. The model correctly predicts the trend that lower  $X$  values cause slightly longer cycle times. However the model doesn't account for the heavy dampening observed in the experiment. Experimental results suggest that higher  $X$  values result in larger oscillations before the valve reaches a stationary position. The valve is also seen to reach a stationary position at the system's positive boundary angle ( $\theta_{b+}$ ) which is different for each tested value of  $X$  as predicted by theory.

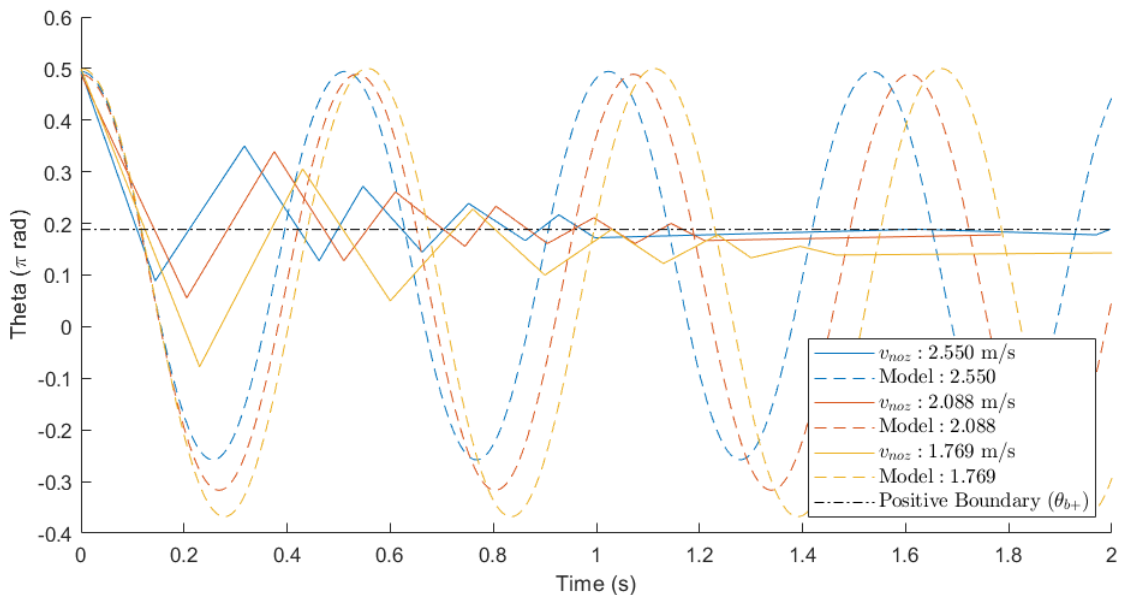


Figure 15: Experimental results compared against model predictions for gravity valve test 1.1 with three different applied  $v_{noz}$  values.

Effectively the gravity valve concept will always experience some sort of damping. Energy losses due to friction in the joint and air resistance are probably (at least partially) responsible for the damping effect. The area of the jet may also play a role, at one point the valve is only subject to a certain area of the jet, this interaction may be responsible for damping effects.

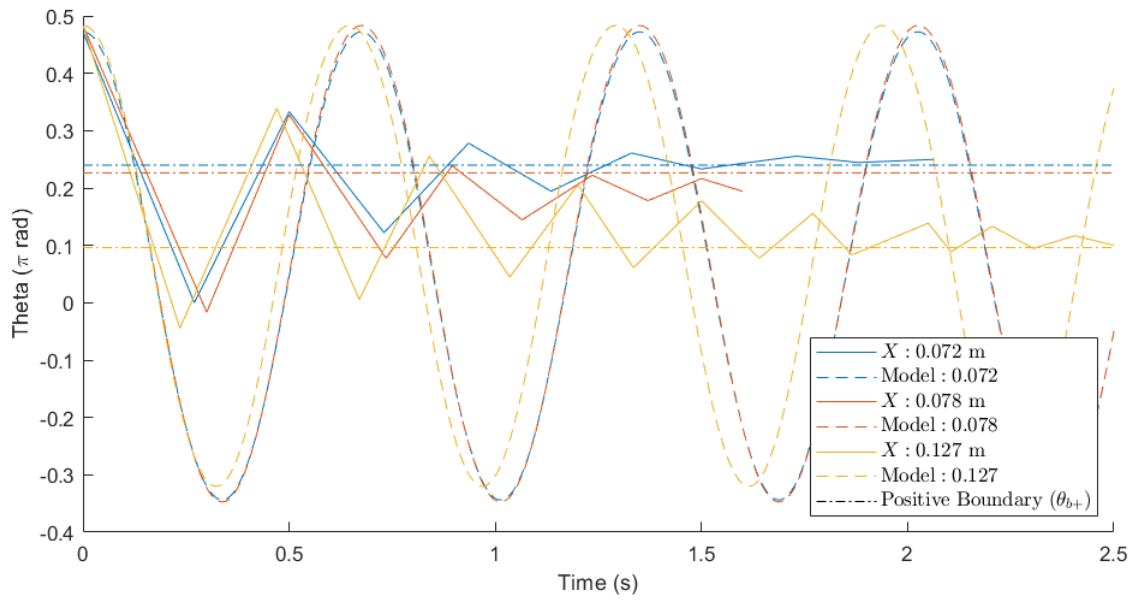


Figure 16: Experimental results compared against model predictions for gravity valve test 2 with different chosen  $X$  values.

## 5.2 Waterwheel Results

### 5.2.1 Waterwheel Analytical Model Results

In this section model parameters influence on waterwheel cycle times and jet open : close ratios are explored. In general method 1 (jet velocity assumption) and method 2 (force considerations) give very similar jet open : close ratio results yet different cycle time results. The tested parameters are different for both waterwheel theory method 1 (the method that assumes the waterwheel rotates at the same velocity as the jet velocity) and method 2 (the method that uses Newtons seconds law and forces applied on the waterwheel blades due to the jet stream).

Method 1 is affected by  $\theta_{noz}$ ,  $X$  and  $L$  values to determine the wheel's rotational angle during which the jet is blocked by a waterwheel blade ( $\theta_j$ ). The only other relevant parameter is  $v_{noz}$  from which the wheel's constant angular velocity is derived from.  $\theta_{noz}$  is kept constant at 20 degrees as required by Deltares, therefore the only tested parameters for method 1 are  $v_{noz}$  and the non dimensional  $L : X$  ratio. Method 2 is also affected by  $\theta_{noz}$ ,  $X$  and  $L$  values to determine the wheels rotational angle during which the jet is blocked by a waterwheel blade ( $\theta_j$ ). In method 2, the wheel's motion is dictated by ( $\tau_{F_n}$ ) and the wheel's moment of inertia ( $I_o$ ) which is used to determine the wheel's angular acceleration as shown in Appendix C.2, Equation (61). From the wheel's angular acceleration, angular velocity and time are derived. Therefore tested parameters for method 2 are the non dimensional jet torque : moment of inertia ratio and  $L : X$  ratio.

As tested parameters are changed to determine their influence on the pulsing water stream, all other system parameters are kept at constant "baseline" values. The constant baseline parameter values are shown in Table 7 and are comparable to the values used in small scale experimental tests on a waterwheel with two blades ( $n = 2$ ). As shown in Table 7, the wheel's deceleration constant when the jet is not in contact with the waterwheel blades ( $njdC$ ) is 0.925. This means when not in contact with the jet, the wheel travels at 0.925 times the angular velocity when it has just left the jet. This value is calibrated based on empirical data, this calibration process is elaborated on in Section 5.2.2.

Table 7: Overview of the baseline parameters used for each waterwheel model test.

Parameter	Default set-up value
$L$ (m)	0.15
$m$ (kg)	0.0485
$X$ (m)	0.15
$OA$ (m)	0.075
$v_{noz}$ (m/s)	2.55
$a$ (m <sup>2</sup> )	0.00007854
$n$	2
$d$ (m)	0.25
$\theta_{noz}$ (deg)	20
$njdC$	0.925

Results for influence of  $v_{noz}$  in waterwheel theory method 1 are shown in Figure 17. As can be seen,  $v_{noz}$  does not affect the open : close ratio whilst a higher jet velocity logically decreases cycle time. This is because a greater jet velocity causes a greater wheel angular velocity resulting in quicker revolutions and thus a reduced cycle time. Effects of the  $L : X$  ratio on method 1 are shown in Figure 18. The ratio is controlled by changing  $X$  whilst keeping  $L$  constant. The lowest possible  $L : X$  ratio is 0.940, any value lower and the jet will not make contact with the waterwheel blades. When the  $L : X$  ratio is between 0.940 - 1 the open : close ratio can increase dramatically from 3.497 to 84.94, satisfying Deltares' requirements. Higher  $L : X$  ratios cause undesirably low open : close ratios in the range of 0 - 1. Regarding cycle time, a lower  $L : X$  ratio results in a higher cycle time.

This is because the radius from the wheel pivot point to the point of jet impact is greater, resulting in a lower angular velocity and thus higher cycle time when converting from linear jet velocity to angular wheel velocity using Equation (57) shown in Appendix C.1.

Results for influence of jet torque : moment of inertia ratio in waterwheel theory method 2 are shown in Figure 19. It doesn't affect the open : close ratio. A greater jet torque ratio results in a lower cycle time. This is because angular acceleration is equal to jet torque divided by wheel moment of inertia, therefore a greater ratio creates a greater angular acceleration resulting in higher angular velocities and lower cycle times. The effect of the  $L : X$  ratio for method 2 is shown in Figure 20, the  $L : X$  ratio is controlled by altering the systems  $X$  value. The jet open : close ratio relation is similar to that of method 1 as it is determined based on the same trigonometric relations that are dependent on  $L$  and  $X$ . Cycle time however differs. A higher  $L : X$  ratio causes a higher cycle time as although the blade spends more time in contact with the jet, the torque due to the jet is less as the distance from waterwheel pivot to jet impact is less. This results in a lower angular acceleration and slower cycle time. However at very low  $L : X$  ratios the effect of the low jet contact time outweighs the higher jet torque magnitudes. The time spent in contact with the jet is so small that jet force acts so infrequently that angular acceleration decreases resulting in higher cycle times.

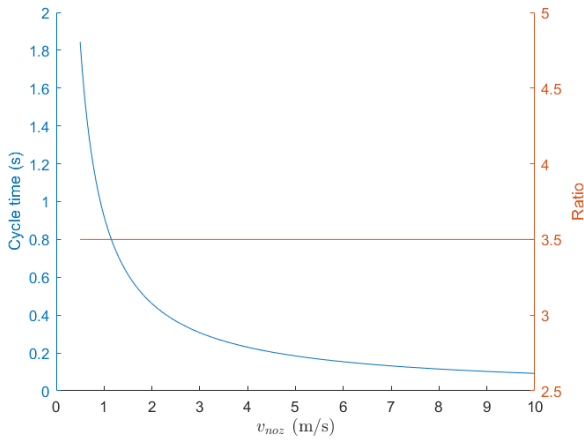


Figure 17: Effect of  $v_{noz}$  on system cycle time and open : close ratio for waterwheel method 1.

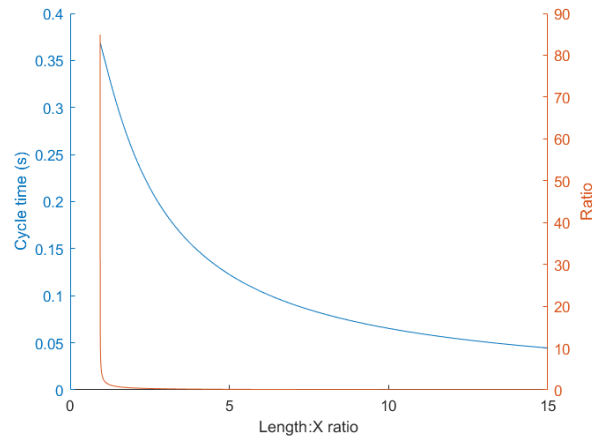


Figure 18: Effect of length :  $X$  ratio on system cycle time and open : close ratio for waterwheel method 1.

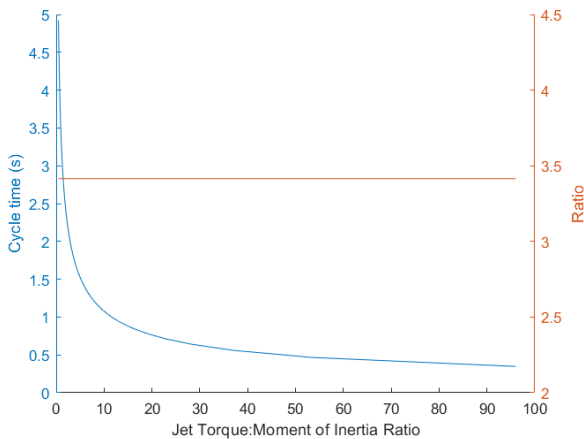


Figure 19: Effect of jet torque : moment of inertia ratio on system cycle time and open : close ratio for waterwheel method 2.

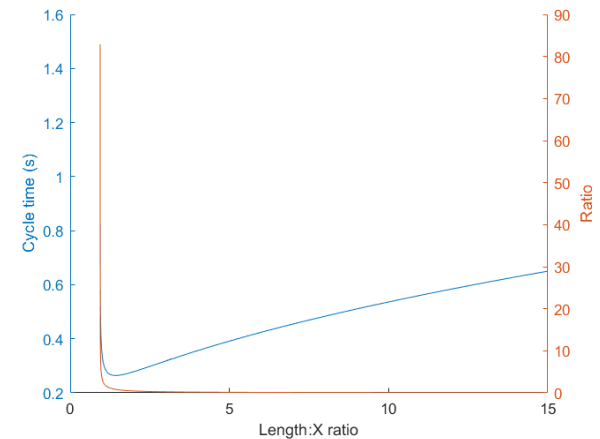


Figure 20: Effect of length :  $X$  ratio on system cycle time and open : close ratio for waterwheel method 2.

### 5.2.2 Waterwheel Experiment Results

In this section waterwheel experimental results are shown and compared to modelling predictions. Experimental observations show that a functional pulsing water stream can be created using the waterwheel method. Initial revolutions are observed to have higher cycle times however a constant cycle time and thus angular velocity appears to be reached after only approximately 12 revolutions. The experiments shown in Table 5 are performed to give insight on the effects of waterwheel blade number ( $n$ ),  $X$ , wheel moment of inertia ( $I_o$ ), valve length ( $L$ ) and nozzle jet velocity ( $v_{noz}$ ). Only cycle time is observed and recorded from the experiments. This is because it was not feasible to accurately measure jet open : close ratio with the available equipment therefore open : close ratio is assumed to only be affected by trigonometry of the waterwheel. Graphed results in Figures 21, 22, 23 and 24 compare experimental results (solid line), method 1 predictions (dotted line) and method 2 predictions (dashed line). Method 1 predictions are shown as a horizontal line as the method only predicts a singular waterwheel angular velocity based on jet vector velocity as explained in Section 2.2.1.

The deceleration constant ( $njdC$ ) used in method 2 is calibrated to 0.925. This means the waterwheel is modelled to rotate at 0.925 times the angular velocity when not in contact with the jet compared to when it was in contact with the jet. Experimental cycle time results from tests 1.1, 1.2, 1.3 and 1.4 as shown in Table 5 are used for calibration. It was difficult to calibrate the model to fit all moment of inertia tests. Therefore the model was calibrated to fit the test with moment of inertia of  $0.000728 \text{ kg m}^2$  because it was the baseline moment of inertia used in most tests. This calibration can clearly be seen in Figure 22 where the model only fits the moment of inertia test of  $0.000728 \text{ kg m}^2$ .

Figure 21 shows results for test 1.1 shown in Table 5. The results show the effect of  $X$  on cycle time of a two bladed waterwheel. Influence of chosen  $X$  values are well predicted by waterwheel modelling method 2. Higher  $X$  values are shown to have higher cycle times due to lower jet contact time.

Figure 22 shows results for test 1.2 shown in Table 5. The results show the effect of waterwheel moment of inertia on cycle time of a two bladed waterwheel. Surprisingly the waterwheel's moment of inertia didn't have an effect upon the eventual cycle time. This contradicts theory set forward by method 2 in which moment of inertia is decisive in determining the wheels angular acceleration.

Figure 23 shows results for test 1.3 shown in Table 5. The results show the effect of  $L$  on cycle time of a two bladed waterwheel. It should be noted that the  $L : X$  ratio is not kept constant for each of the three  $L$  value test due to practical difficulty in doing so. These varying  $L : X$  values may interfere with the true impact of  $L$ . Nevertheless, higher  $L$  values are shown to result in larger cycle times as predicted by both models.  $L$  values of 0.15 m and 0.2 m are well approximated by method 2 however the cycle time for  $L = 0.25$  m is underestimated by method 2.

Figure 24 shows results for test 1.4 shown in Table 5. The results show the effect of  $v_{noz}$  on cycle time of a two bladed waterwheel. The experiment suggests  $v_{noz}$  has a strong effect upon cycle time, lower  $v_{noz}$  values result in higher cycle times. The influence on cycle time is not proportional to  $v_{noz}$  however as the lower  $v_{noz}$  value of 1.769 m/s has a disproportionately larger cycle time compared to the tests with  $v_{noz}$  values of 2.55 and 2.088 m/s.

Waterwheel cycle times appear to be very quick and unrealistic to mimic wave erosion action (in the 0.15-0.4 second range). Therefore a braking system was tested to see if it was possible to increase cycle times. This braking system was very primitive and simply consisted as a fixed stick applying friction to the three bladed waterwheel as shown in Appendix F, Figure 32. Figure 25 shows cycle time results for a three bladed wheel exposed to a jet with velocity of 2.55 m/s compared to cycle

results for the same wheel with the braking system applied (The first tests of both test 2.1 and 2.2 as shown in Table 5). The braking system achieves a 32.4% increase in cycle time thus proving the potential to increase cycle times if desired.

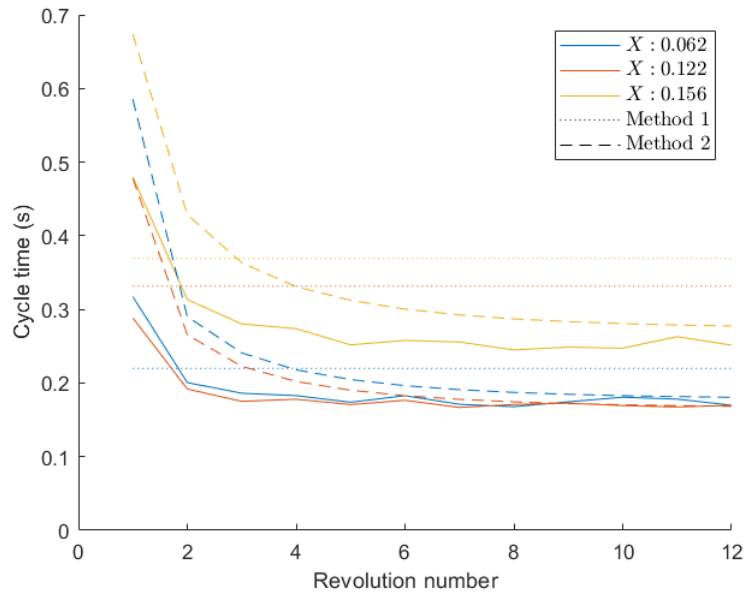


Figure 21: Experimental results of test 1.1, a two bladed waterwheel with three different chosen  $X$  values. Results are compared against method 1 (jet velocity model) and method 2 (force model) predictions.

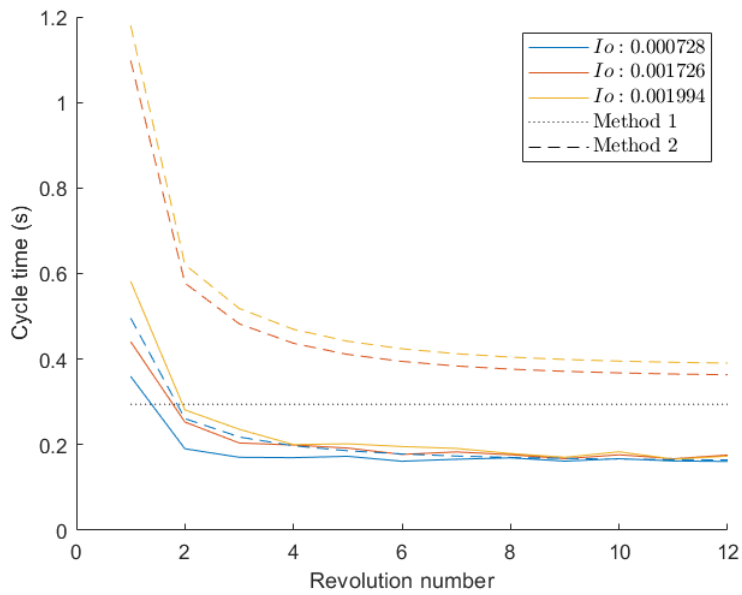


Figure 22: Experimental results of test 1.2, a two bladed waterwheel with three different water wheel moment of inertia values. Results are compared against method 1 (jet velocity model) and method 2 (force model) predictions.

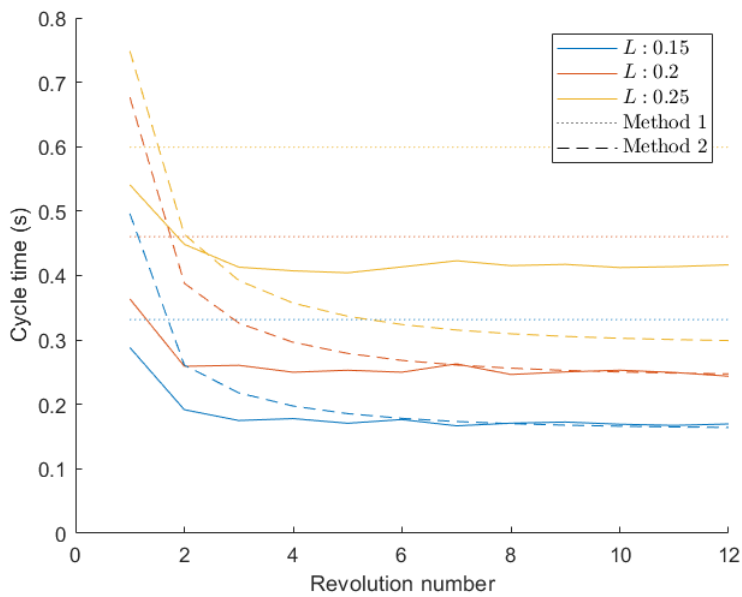


Figure 23: Experimental results of test 1.3, a two bladed waterwheel with three different  $L$  values. Results are compared against method 1 (jet velocity model) and method 2 (force model) predictions.

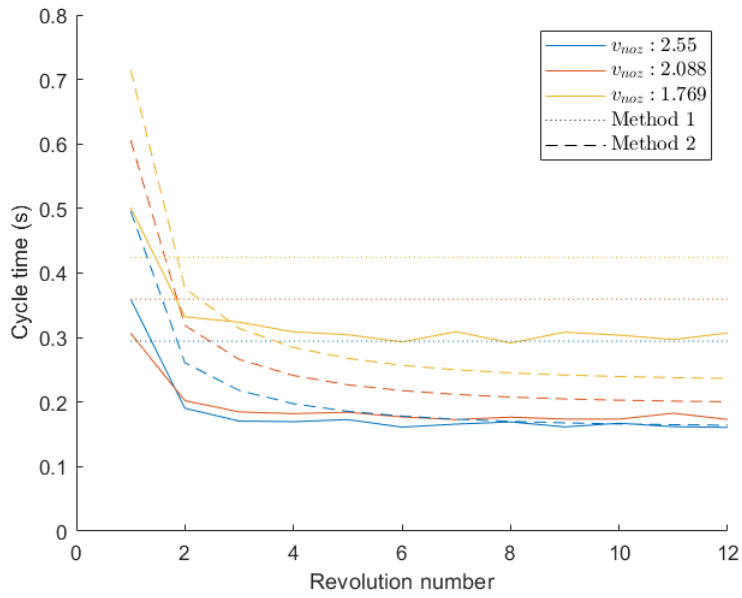


Figure 24: Experimental results of test 1.4, a two bladed waterwheel with three different applied  $v_{noz}$  values. Results are compared against method 1 (jet velocity model) and method 2 (force model) predictions.

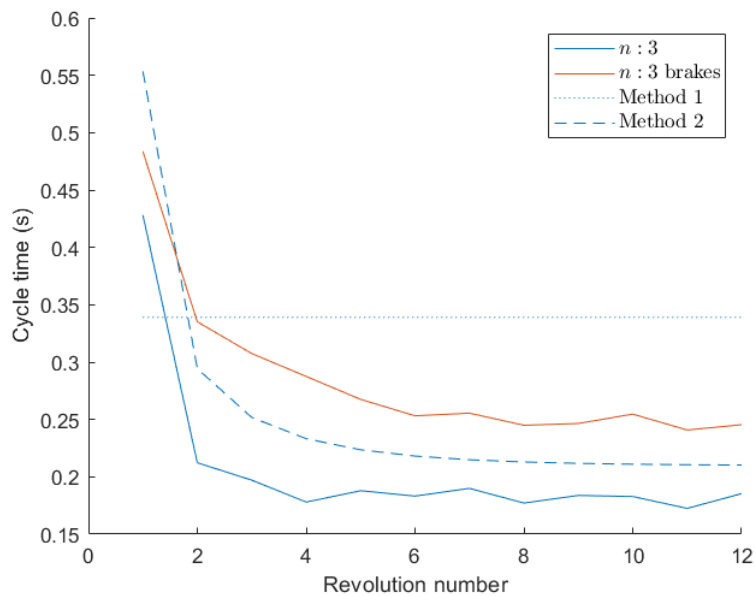


Figure 25: Experimental results for waterwheel with three blades with and without brake system applied. Results are compared against method 1 (jet velocity model) and method 2 (force model) predictions.

## 6 Discussion

In this section results for both the gravity valve and waterwheel concepts are discussed and critically reflected upon. Potential improvements to theoretical and experimental procedures and reasons for theoretical and empirical discrepancies are also given.

### 6.1 Gravity Valve Discussion

According to the gravity valve model a stationary situation is never reached, this is contrary to experimental data where the valve reaches a stationary situation after only 4-5 swing cycles at the positive theta boundary (shown in Figure 5). This could be attributed to the models theoretical understanding being purely based upon Newtonian mechanics. As a result only general movements are considered and small yet potentially significant details are overlooked. The lack of dampening in the model could also be attributed to ignoring energy losses due to joint friction, air resistance and weather conditions. Another reason for the observed dampening effect could be that because the jet has an area, at the positive boundary (the border between the valve being in or out of contact with the jet), the jet is only partially impacting the valve, this reduced jet torque could attribute to a dampening effect. Due to not being able to model dampening effects the model has limited ability to answer the main question of whether the concept will actually work. Nevertheless it can give valuable insight into how input parameters influence system performance and what additional measures are required to realise a working system.

Regarding the non-dimensional parameters, it is difficult to isolate each parameter. For example jet:weight torque ratio is dependent on a multitude of factors, namely;  $\rho, a, v, X, L, m, g, OA, \theta_{noz}$  and  $\theta$ . In this report  $m$  was chosen to control the ratio however this also effects the moment of inertia. Altering the  $L:X$  and  $L:OA$  ratios also changes the jet:weight torque ratio therefore it is difficult to say to what extent each non dimensional parameter effects system performance as jet:weight torque ratio cannot be kept constant. It can be concluded however that based on theoretical and empirical results the jet:weight torque ratio is the most influential parameter, this is logical as jet and weight torques determine angular acceleration which ultimately dictates valve movement over time. The  $\theta_{start}$  value only influences theta positive and negative boundaries, the  $L:X$  ratio influences theta positive and negative boundaries and only partially the jet torque and and the  $L:OA$  ratio influences the moment of inertia and only partially the weight torque.

The model could be improved by incorporating some sort of energy loss or dampening function, this function could be in the form of reduction in swing angle per swing cycle or reduction in angular velocity and thus kinetic energy over time. The function can be derived based on a large amount of empirical data and is likely dependent on system parameters, this is hinted at by experimental results in Figure 16 showing setups with higher  $X$  values oscillating longer and thus losing energy slower. Once the energy loss function is incorporated into the model, the model can be used as a tool to test concept variations. It is highly likely that some form of external force such as a magnet is required to account for dampening effects to avoid a stationary condition.

The gravity valve experiment could be improved by conducting multiple repeats of each test and taking the average value. Despite taking much longer to process results (due to having to re-watch and process more footage) taking average results would improve reliability of each cycle time result and would help limit anomalies. This would make parameter influence trends more distinguishable and reliable. The experiment could also be improved by conducting it in a laboratory with improved equipment to gain more reliable system parameter measurements. A laser could be used to measure the valves movement. This will improve accuracy, provide continuous valve position measurements in oppose to only recording valve swinging peaks, reduce experiment time as videos don't have to be painstakingly analysed afterwards and the jet open:close ratio could be measured from the continuous data.

## 6.2 Waterwheel Discussion

Method 2 matches experimental results better than method 1. Method 1 consistently overestimates cycle time, the method assumes the waterwheel moves at an angular velocity equal to that of the jet streams vector velocity as explained in Section 2.2.1. Angular velocity changes as the wheel rotates during the jet - wheel blade impact period, therefore the average angular velocity is taken. The method could be improved by taking the maximum angular velocity of the water during the impact period or by considering velocity increase of the water due to conversion of gravitational potential energy into kinetic energy. The latter phenomenon was explored for both the gravity valve and waterwheel concepts. Bernoulli's equation was used to derive an equation relating impact velocity to theta as shown in Appendix G. The equation is complex and would need to be integrated within integrals for angular velocity and time functions. This process is labour intensive and is not seen as necessary due to the system's small horizontal distance from nozzle to valve ( $d$ ) and high velocities leading to negligible differences between jet velocity at the nozzle and jet velocity at impact. For example, a nozzle velocity of 7 m/s has an impact velocity of 7.17 m/s when  $X$  is 0.2 m and  $d$  is 0.25 m. Therefore theory throughout this report has used the assumption that impact velocity equals nozzle velocity.

The biggest pitfall in method 2 is that its theoretical understanding considers waterwheel acceleration and thus cycle time to be dependent on waterwheel moment of inertia, as derived from Newton's angular second law. Experimental data shows that waterwheel moment of inertia appears to have no effect on cycle time, this observation could be explained by saying heavier wheels have greater momentum, this greater momentum reduces the amount in which the wheel decelerates when not in contact with the jet, increasing angular velocity. This increased velocity is cancelled out by greater moment of inertia's greater resistance to angular motion thus resulting in the same angular velocities and cycle time regardless of the waterwheels moment of inertia. This discrepancy weakens method 2's ability to predict cycle times of up-scaled systems where wheels have higher moment of inertia's. However based on experimental data, it cannot be certain that moment of inertia has no effect on cycle time as only three similar moment of inertia's were tested due to equipment limitations. More tests on a larger range of moment of inertia's is required to confirm this observation.

Method 2 accurately models general trends caused by changing  $v_{noz}$ ,  $X$  and  $L$  values. Some model predictions, namely setups when  $v_{noz}$  is equal to 1.769 m/s (Figure 24) and when  $L$  is 0.25 m (Figure 23) deviate from experimental results however this can be attributed to the sensitivity of error in experimental measurements. For example, when  $v_{noz}$  is 1.769 m/s cycle time is measured as 0.307 seconds whilst the model predicts a time of 0.237 s. However if  $v_{noz}$  is measured as 1.400 m/s the model predicts a cycle time of 0.304 s in line with experimental observations. The small error margin in jet velocity measurements could have been caused by the basic measuring equipment and apparatus used. The same is the case for the set up when  $L$  is 0.25 m where empirical results show a cycle time of 0.417 seconds. The model predicts a cycle time of 0.290 s when  $X$  is measured as 0.254 m. If  $X$  is measured as 0.265 m the model predicts a cycle time of 0.406 s. This demonstrates the sensitivity and potential inaccuracy of the experimental measurements. As  $X$  is measured from camera footage, camera perspective could be responsible for errors in  $X$  measurements.

Calibration of method 2's no-jet deceleration constant ( $n_{jdC}$ ) was difficult as it was impossible to fit the model to all data recorded from tests 1.1, 1.2, 1.3 and 1.4 as shown in Table 5. A calibration factor dependent on system  $I_o$ ,  $n_{noz}$ ,  $X$  and  $L$  values would have been required but is hard to implement. Thus a simple constant is chosen to model angular velocity decrease and is calibrated to 0.925. This weakens the models robustness as it is calibrated to fit only a select few system set-ups, in this case the constant is calibrated to fit one of the three moment of inertia tests. A larger set of experimental data and more complex deceleration functions are required to reliably calibrate and model wheel deceleration when not in contact with the jet..

The braking system used during the experiment was very primitive and simply demonstrated feasibility of braking system that applies friction. It is unknown whether a braking system will be able to achieve an increase in cycle time from 0.2 seconds to the desired range of 1 - 6 seconds. Another issue to note is that when performing braking system tests, friction will have to be kept the same for each test repeat, it may be difficult to replicate the same frictional values as friction reduces over time and test setups may be sensitive and complex.

Non-dimensional parameters being interconnected remains an issue for the waterwheel method 2. Jet torque : moment of inertia ratio dictates the angular acceleration magnitude whereas  $L : X$  ratio dictates the boundaries in which the waterwheel is in contact with the jet ( $\theta_j$ ) as well as dictating jet open : close ratios. Sadly the  $X$  value also influences jet torque magnitude, therefore the influence of each individual parameter cannot be explicitly determined as when altering  $X$  for the  $L : X$  ratio jet torque is not kept constant. In hindsight  $L : X$  ratio should have been altered by keeping  $X$  constant and altering  $L$  whilst retaining the same moment of inertia, this way jet torque : moment of inertia ratio is kept constant and the true effect of  $L : X$  ratio can be determined. It would also have been insightful to convert experimental results, for example cycle time results for three different  $v_{noz}$  values as shown in Figure 24, into non-dimensional jet torque : moment of inertia ratios. Therefore model predictions for non-dimensional parameter trends such as the one shown in Figure 19, can be verified with experimental data. The issue is that only three different  $V_{noz}$  values are tested, making it difficult to reliably verify trends and confirm which non dimensional parameter is the most influential. A large variety of jet torque : moment of inertia ratio experiments should be performed to reliably verify model trend predictions.

The parameter with the greatest impact on jet open : close ratio is the  $L : X$  ratio. As mentioned in the results section the  $L : X$  ratio is very sensitive between 0.940 and 1. Within this range the open : close ratio can increase dramatically from 3.497 to 84.94. This is because at high values of  $X$  the extent of which the jet is in contact with the valve is very sensitive. It must be noted that the chosen  $\theta_{noz}$  value effects the sensitivity of the  $L : X$  ratio. In this report  $\theta_{noz}$  is taken as 20 degrees to match Deltares' desired setup. If greater  $\theta_{noz}$  values are taken and providing the  $L : X$  ratio is kept constant, the angle in which the wheel is in contact with the jet ( $\theta_j$ ) increases, this reduces the jet open : close ratio and cycle times. Due to these drastically reduced open : close ratios and cycle times sensitivity of the  $L : X$  ratio is reduced. A non-dimensional parameter that considers  $L$ ,  $X$  and  $\theta_{noz}$  expressed in percentage of the revolution in which the jet is blocked is a more informative parameter that considers different  $\theta_{noz}$  values.

## 7 Recommendation to Deltares

Based on the theory and empirical observations, the gravity valve method is not recommended and appears to be infeasible as it always reaches a stationary condition. Changes in input parameters can limit this dampening effects such as increasing the  $X$  value however eventually a stationary condition will always be reached. Future research could be conducted to determine exactly what causes this heavy dampening effect and to confirm whether the concept is actually infeasible. This could be achieved by employing dynamic modelling to understand the interaction between the jet stream and the valve and by modelling energy losses. As mentioned in the discussion an energy loss function could also be incorporated into the model from which concept alterations can be tested, for example concepts that use input force such as magnets to avoid dampening.

It is recommended Deltares uses or further explores a two bladed waterwheel to create the desired pulsing water stream. Two bladed waterwheels have higher and more desirable jet open : close ratios when compared to three and four bladed waterwheels. Physical experiments showed that a lasting pulsing stream can be achieved. Theory and modelling of waterwheel method 2 provided dependable results. Desired jet open : close ratios between 4 to 20 can be achieved with  $L : X$  ratios between 0.943 and 0.991. At these ratios  $X$  becomes very sensitive and the jet should not be considered as a straight beam. The parabolic trajectory of the jet stream should be accounted for to achieve the desired jet open : close ratio and to ensure the jet stream does not miss the waterwheel blades entirely. It is recommended to develop some sort of braking system as cycle time of a two bladed waterwheel with blade length 0.2 m, wheel mass 4 kg and blade centre of mass 0.1 m subjected to the fire hoses full scale jet stream is modelled to be 0.0606 seconds, well below the desired time of 1-6 seconds. It is experimentally proven that braking systems can increase pulsing periods. A braking system gives more freedom to choose desired blade lengths and masses for practicality. The system can also be used to adjust pulsing times accordingly, for example wind could interfere with the waterwheel, the braking system could then be adjusted to achieve the desired pulse time for experiment continuity. Either a frictional braking system or a system in the form of a bike chain and gears could be an option. If the latter is chosen, cycle time can be influenced by the chosen gear.

More extensive small scale waterwheel tests should be performed to identify clear reliable trends of non-dimensional parameter effects. It is especially important to determine whether the waterwheel's moment of inertia has an effect upon cycle time, from these trends the model proposed in this report can be either calibrated or rejected. The model can be used to predict waterwheel cycle time for Deltares' full scale system, from which the amount of friction or gear resistance required from the braking system to achieve desired cycle times can be determined. Experimental measuring of the jet open : close ratio should also be done to confirm whether the trigonometric model assumptions and predictions for open : close ratios hold.

## 8 Conclusion

This study explored the feasibility of both the gravity valve and waterwheel concepts to create a pulsing water stream for use in Deltares' fire hose method. Theoretical principles were applied to create analytical models used to assess feasibility and the influence of system parameters on the pulsing stream's cycle times and jet open:close ratios. Physical experiments were performed and their results were compared to model predictions to help provide Deltares with a recommendation for future research directions and how to realise a pulsing water stream system.

The gravity valve concept (illustrated in Figure 26) appears to be infeasible as based on experimental results, dampening occurs and a stationary situation is always reached as the valve comes to rest at the positive boundary (the boundary between valve - jet contact and no contact). As a result a pulsing stream is not created as the valve continuously blocks the stream. This is presumably due to energy losses, it could also be that at some point during the swing cycle, the jet area only partially acts on the valve, reducing angular velocity and encouraging dampening. Future research would be required to specifically identify what is causing the heavy dampening effects observed in the physical experiment. A two-bladed waterwheel concept is found to be the most viable option for Deltares, two blades coupled with a  $L : X$  ratio between 0.943 and 0.991 helps achieve Deltares' desired jet open:close ratio between 4 and 20 when the nozzle angle is kept at 20 degrees to the horizontal. The waterwheel concept as well as the mentioned  $L$  and  $X$  parameters are illustrated in Figure 26. The issue is that the system cycle time is in the order of 0.1 seconds, well below the desired time of 1-6 seconds. However in this project it was proven experimentally that a frictional braking system can prolong the cycle time therefore a braking system should be researched to achieve cycle times in the desired 1-6 second range. A possible braking system could involve attaching the waterwheel to a bike chain and gears, gears could then be selected to dictate cycle times.

Two theoretical methods were used to model the waterwheel's cycle time and jet open:close ratios. Method 1 assumes the waterwheels spins at a constant angular velocity is equal to that of the jet velocity. Method 2 considers forces acting upon the system and uses the angular version of Newtons second law to derive equations for waterwheel angular acceleration, angular velocity and time with respect to the waterwheels rotational angle, theta. Method 2 better matches experimental results however its theoretical understanding still contains uncertainties and assumptions. The main assumption is that the wheel is assumed to decelerate when not in contact with the jet. The extent of deceleration is modelled using a deceleration constant which is calibrated based on limited experimental measurements. The deceleration constant is too inflexible to be calibrated to match all experimental results therefore a deceleration function based on system parameters and more experimental data should be researched to better model the waterwheel system.

Generally waterwheel method 2 performs well when compared to experimental results. It correctly predicts that the waterwheel angular velocity increases until it converges at an optimal velocity. It also predicts trends of changing  $L$ ,  $v_{noz}$  and  $X$  values. Greater  $L$  values result in higher cycle times, greater  $v_{noz}$  values result in lower cycle times and smaller  $X$  values result in greater cycle times. However very large  $X$  values can also result in much larger cycle times and jet open:close ratios as desired by Deltares as the blade is in contact with the jet stream for such a short period of time.  $X$  becomes a very sensitive parameter with regards to the jet open:close ratio at large values. The main discrepancy between theoretical understanding and experimental results is that it was observed experimentally that the waterwheel's moment of inertia does not effect cycle time. More extensive physical experiments should be performed to confirm whether moment of inertia really does not effect wheel cycle time.

Deltares' full scale system should have an  $L : X$  ratio between 0.943 and 0.991 to achieve the desired jet open:close ratio of 4 - 20 when nozzle angle is kept at 20 degrees to the horizontal ( $\theta_{noz}$ ). Greater  $\theta_{noz}$  values drastically reduce the jet open:close ratio, in hindsight a non dimensional parameter

incorporating  $L$ ,  $X$  and  $\theta_{noz}$  would have been more versatile. A braking system should be applied to help achieve desired cycle times of 1 - 6 seconds. The only issue is that cycle times should be predicted to determine how much braking force to apply. A prediction for cycle times cannot be given because it is not certain whether waterwheel moment of inertia effects cycle time, limited experimental results show moment of inertia having no effect on cycle time. Moment of inertia is decisive in determining cycle time in waterwheel method 2 as it determines waterwheel angular acceleration. If moment of inertia appears to be redundant in influencing cycle time, waterwheel method 2 cannot be used to predict cycle times. More experiments should be performed on a wider range of waterwheel moment of inertia's to determine whether moment of inertia is influential. It is proven experimentally and theoretically however that torque due to jet force and  $L : X$  ratio does influence cycle time, greater torque causes reduced cycle times and greater  $L : X$  ratios cause greater cycle times, except if  $L : X$  is sufficiently small (0.94 - 1.3), then greater cycle times are achieved due to such small waterwheel blade and jet contact time. This relationship is illustrated in the graph shown in Figure 27.

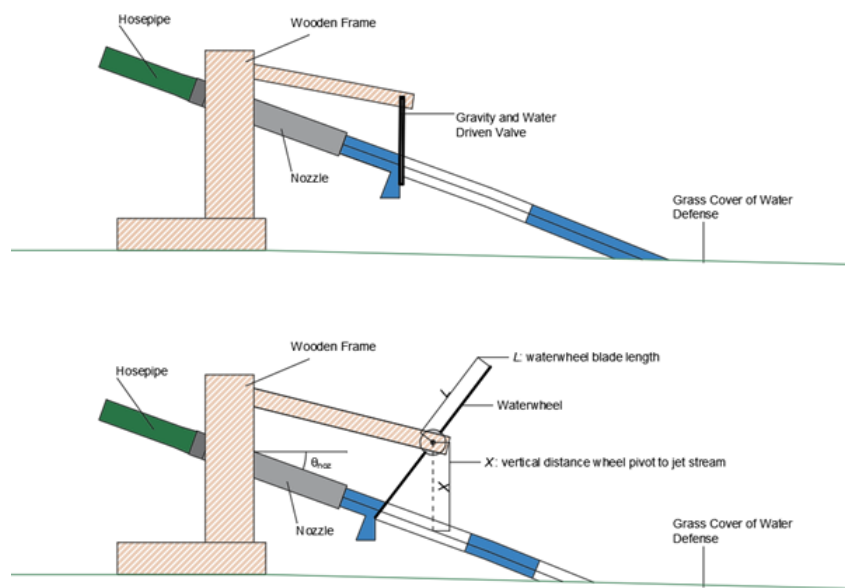


Figure 26: Illustration of the gravity valve concept (above) and the waterwheel concept and its defined  $L$  and  $X$  parameters (below).

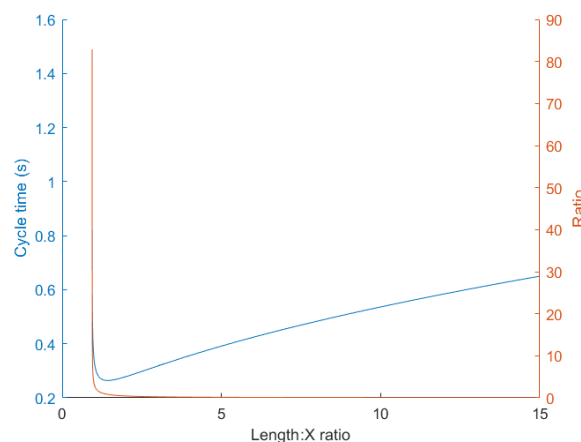


Figure 27: Effect of blade length :  $X$  ratio on system cycle time and open : close ratio for waterwheel method 2.

## References

- Briaud, J. L., Shafii, I., Chen, H. C., and Medina-Cetina, Z. (2019). Relationship between erodibility and properties of soils. *National Academies of Sciences, Engineering, and Medicine*.
- Hoffmans, G., van Hoven, A., Steendam, G. J., and van der Meer, J. (2018). Summary of research work about erodibility of grass revetments on dikes. Technical report, Deltares.
- Jak, M. and Kok, M. (2000). A database of historical flood events in the netherlands. [https://www.researchgate.net/publication/253205466\\_A\\_Database\\_of\\_Historical\\_Flood\\_Events\\_in\\_the\\_Netherlands](https://www.researchgate.net/publication/253205466_A_Database_of_Historical_Flood_Events_in_the_Netherlands). Accessed April 15, 2021.
- Rijkswaterstaat. (2010). Water act. <https://www.helpdeskwater.nl/secundaire-navigatie/english/@176675/dutch-water-act/>. Accessed April 15, 2021.
- Rijkswaterstaat. (2012). Flood risk and water management in the netherlands. <https://www.helpdeskwater.nl/secundaire-navigatie/english/@178463/flood-risk-and-water/>. Accessed April 15, 2021.
- Trung, H. L., Verhagen, H. J., and Vrijling, J. K. (2016). Damage to grass dikes due to wave overtopping. *Natural Hazards*, pages 849–875.
- van Alphen, J. (2015). The delta programme and updated flood risk management policies in the netherlands. *Journal of Flood Risk Management/ Volume 9, Issue 4.*, pages 310–319.
- van Bergeijk, V. M., Verdonk, V. A., Warmink, J. J., and Hulscher, S. J. (2021). The cross-dike failure probability by wave overtopping over grass-covered and damaged dikes. *Water*, 13, page 690.
- van Bergeijk, V. M., Warmink, J. J., and Hulscher, S. J. (2020). Modelling the wave overtopping flow over the crest and the landward slope of grass-covered flood defences. *Journal of Marine Science and Engineering*, 8., page 489.
- van der Most, H., Tánčzos, I., de Bruijn, K. M., and Wagenaar, D. (2014). New, risk-based standards for flood protection in the netherlands. Technical report, Deltares.
- van Steeg, P. and Mourik, G. (2020). Ontwikkeling brandslangmethode. Technical report, Deltares.
- Voorendt, M. Z. (2015). The development of the dutch flood safety strategy. Technical report, TUDelft.
- Warmink, J. J., van Bergeijk, V. M., Frankena, M., van Steeg, P., and Hulscher, S. J. (2020). Modelling transitions in grass covers to quantify wave overtopping erosion. *Costal Engineering Proceedings 2020*.
- Wesselink, A. J., Bijk, W. E., de Vriend, H. J., and Krol, M. S. (2007). Dutch dealings with the delta. *Nature Culture* 2., pages 188–209.

# Appendices

## A Gravity Valve Theory Calculations

In this section detailed calculations used in the gravity valve theory are shown. Firstly required dependent variables as shown in Figure 2 are calculated from input parameters using trigonometry. The jet-valve impact angle when the valve is vertical can be derived from the nozzle angle.

$$\theta'_v = \frac{\pi}{2} - \theta_{noz} \quad (8)$$

A general formula for the jet-valve impact angle can be derived based on the valves current angle ( $\theta$ ) and the jet-valve impact angle when the valve is vertical from Equation (8).

$$\theta' = \theta'_v - \theta \quad (9)$$

The distance  $OB$  which is the length from the pivot to where the jet force is acting is found using the sine rule.

$$OB = \frac{X \sin(\pi - \theta'_v)}{\sin(\theta')} = \frac{X \sin(\pi - \theta'_v)}{\sin(\theta'_v - \theta)} \quad (10)$$

Negative and positive boundary angles are defined as shown in Figure 3. Both boundaries can be derived using the sine rule from triangles shown in Figure 28.

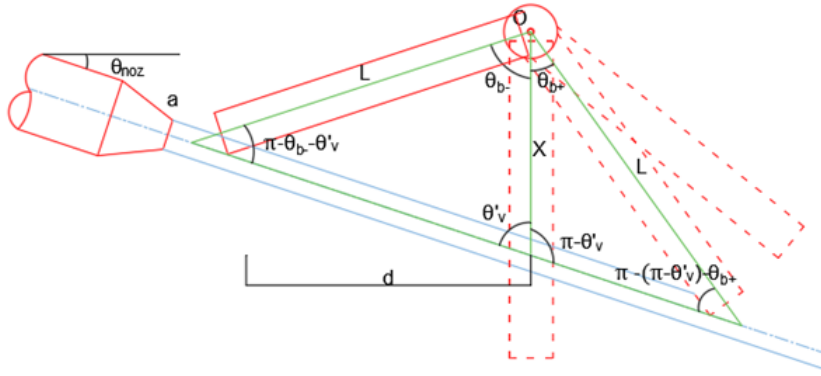


Figure 28: Trigonometric relations used to derive both the gravity valve's positive and negative boundaries.

$$\theta_{b+} = \theta'_v - \sin^{-1}\left(\frac{X \sin(\pi - \theta'_v)}{L}\right) \quad (11)$$

$$\theta_{b-} = \pi - \theta'_v - \sin^{-1}\left(\frac{X \sin(\theta'_v)}{L}\right) \quad (12)$$

Next force normal to the valve due to the jet stream is found using the impulse momentum principle as shown in Equation (13). Torque exerted on the valve around pivot point  $O$  due the jet and weight force are calculated in Equations (14) and (15) respectively by multiplying force by perpendicular distance to pivot. Interestingly it should be noted that when applied, torque due to jet force ( $\tau_{F_n}$ ) is constant no matter what value  $\theta$  is.

$$F_n = \rho a v^2 \sin(\theta') = \rho a v^2 \sin(\theta'_v - \theta) \quad (13)$$

$$\tau_{F_n} = F_n OB = \rho a v^2 \sin(\theta'_v - \theta) \frac{X \sin(\pi - \theta'_v)}{\sin(\theta'_v - \theta)} = \rho a v^2 X \sin(\pi - \theta'_v) \quad (14)$$

$$\tau_{mg} = mg O A \sin(\theta) \quad (15)$$

Next the angular version of Newton's second law ( $F=ma$ ) is shown in Equation (16), where  $\sum \tau_o$  is the summation of torque,  $I_o$  is the valve's moment of inertia from the pivot point and  $\alpha$  is the angular acceleration.

$$\sum \tau_o = I_o \alpha \quad (16)$$

The valve's instantaneous angular acceleration with respect to  $\theta$  can be found by rearranging Equation (16) as shown in Equation (17).

$$\alpha = \frac{\sum \tau_o}{I_o} \quad (17)$$

From angular acceleration, angular velocity in terms of  $\theta$  can be determined by substituting the relation for  $\omega$  shown in Equation (19) into the relation for  $\alpha$  shown in Equation (18). The relation for  $\omega$  in terms of  $\theta$  is shown in Equation (20).

$$\alpha = \frac{d\omega}{dt} = \frac{d\omega}{d\theta} \times \frac{d\theta}{dt} \quad (18)$$

$$\omega = \frac{d\theta}{dt} \quad (19)$$

$$\alpha = \frac{d\omega}{d\theta} \times \omega \longrightarrow \alpha d\theta = \omega d\omega \quad (20)$$

Next, time can be found in terms of  $\theta$  using the relationship shown in Equation (21).

$$\omega = \frac{d\theta}{dt} \longrightarrow \omega dt = d\theta \longrightarrow \frac{1}{\omega} d\theta = dt \quad (21)$$

In sections A.1, A.2 and A.3, Equations for instantaneous angular acceleration ( $\alpha$ ), angular velocity ( $\omega$ ) and time ( $t$ ) at any given value of  $\theta$  are derived for each of the three cycle phases. The three phases are; phase 1; when only the weight force acts, phase 2; when jet force and weight force act and phase 3; when jet force and weight force act when theta is negative.

### A.1 Phase 1: Only Weight Force Acting

Using Equation (17) angular acceleration for phase 1 ( $\alpha_1$ ) can be determined as shown in Equation (22):

$$\alpha_1 = \frac{-\tau_{mg}}{I_o} = \frac{-mgOAsin(\theta)}{I_o} \quad (22)$$

Next using the relationship shown in Equation (20) angular velocity can be determined by solving the integral shown in Equation (23). The evaluated integral is shown in Equation (25) where  $\theta_i$  and  $\omega_i$  are the initial angle and angular velocity values.

$$\int_{\theta_i}^{\theta} \frac{-mgOAsin(\theta)}{I_o} d\theta = \int_{\omega_i}^{\omega} \omega d\omega \quad (23)$$

$$\left[ \frac{mgOAcos(\theta)}{I_o} \right]_{\theta_i}^{\theta} = \left[ \frac{\omega^2}{2} \right]_{\omega_i}^{\omega} \quad (24)$$

$$\omega_1 = \left( \frac{2(mgOAcos(\theta) - mgOAcos(\theta_i))}{I_o} + \omega_i^2 \right)^{0.5} \quad (25)$$

Next using the relationship shown in Equation (21) time can be determined by solving the integral shown in Equation (26). The integral is too complex to be expressed in elementary functions in

subsequent phases and thus the Equation for time shown in Equation (27) is determined numerically using MATLAB.

$$\int_{\theta_i}^{\theta} \frac{1}{\left(\frac{2(mgOAcos(\theta)-mgOAcos(\theta_i))}{I_o} + \omega_i^2\right)^{0.5}} d\theta = \int_{t_i}^t dt \quad (26)$$

$$t_1 = \int_{\theta_i}^{\theta} \frac{1}{\left(\frac{2(mgOAcos(\theta)-mgOAcos(\theta_i))}{I_o} + \omega_i^2\right)^{0.5}} d\theta + t_i \quad (27)$$

## A.2 Phase 2: Jet Force and Weight Force Acting

The same process is applied for phase two, except this time the summation of torque is different as now torque due to the water jet is also acting. Angular acceleration is determined as shown in Equation (28).

$$\alpha_2 = \frac{\tau_{F_n} - \tau_{mg}}{I_o} = \frac{\rho av^2 X \sin(\pi - \theta'_v) - mgOAsin(\theta)}{I_o} \quad (28)$$

From the angular acceleration the integral for  $\omega$  shown in Equation (29) is evaluated to get the Equation for  $\omega_2$  as shown in Equation (31).

$$\int_{\theta_i}^{\theta} \frac{\rho av^2 X \sin(\pi - \theta'_v) - mgOAsin(\theta)}{I_o} d\theta = \int_{\omega_i}^{\omega} \omega d\omega \quad (29)$$

$$\left[ \frac{\rho av^2 X \sin(\pi - \theta'_v)\theta + mgOAcos(\theta)}{I_o} \right]_{\theta_i}^{\theta} = \left[ \frac{\omega^2}{2} \right]_{\omega_i}^{\omega} \quad (30)$$

$$\omega_2 = \left( \frac{2((\rho av^2 X \sin(\pi - \theta'_v)\theta + mgOAcos(\theta)) - (\rho av^2 X \sin(\pi - \theta'_v)\theta_i + mgOAcos(\theta_i)))}{I_o} + \omega_i^2 \right)^{0.5} \quad (31)$$

The integral for time which will be numerically integrated using MATLAB is shown in Equation (32).

$$t_2 = \int_{\theta_i}^{\theta} \frac{1}{\left(\frac{2((\rho av^2 X \sin(\pi - \theta'_v)\theta + mgOAcos(\theta)) - (\rho av^2 X \sin(\pi - \theta'_v)\theta_i + mgOAcos(\theta_i)))}{I_o} + \omega_i^2\right)^{0.5}} d\theta + t_i \quad (32)$$

### A.3 Phase 3: When theta is negative

When theta is negative some trigonometric relations change affecting Equations for  $\tau_{mg}$ , both  $\tau_{F_n}$  and  $\tau_{mg}$  also now act in the positive direction. The relation for valve impact angle at vertical valve ( $\theta'_v$ ) and valve impact angle ( $\theta'$ ) remain the same. Relations for  $OB$  and  $F_n$  and thus  $\tau_{F_n}$  remain the same as  $\sin(\pi - x) = \sin(x)$ . This relation relation is explained below.

$OB$  changes due to trigonometry and the applied sine rule.

$$OB = \frac{X \sin(\theta'_v)}{\sin(\pi - \theta')} = \frac{X \sin(\theta'_v)}{\sin(\pi - (\theta'_v - \theta))} \quad (33)$$

$F_n$  changes due to trigonometry, the sin angle is either  $\theta'$  or  $\pi - \theta'$  depending on the valves angle, nevertheless,  $\sin(\theta)$  is equal to  $\sin(\pi - \theta)$  so the value is not affected.

$$F_n = \rho av^2 \sin(\pi - \theta') = \rho av^2 \sin(\pi - (\theta'_v - \theta)) \quad (34)$$

The resulting equation for  $\tau_{F_n}$  is shown in Equation (35).

$$\tau_{F_n} = F_n OB = \rho av^2 \sin(\pi - (\theta'_v - \theta)) \frac{X \sin(\theta'_v)}{\sin(\pi - (\theta'_v - \theta))} = \rho av^2 X \sin(\theta'_v) \quad (35)$$

Regarding  $\tau_{mg}$ , due to trigonometry  $\theta$  becomes minus  $\theta$  as shown in Equation (36).

$$\tau_{mg} = mg O A \sin(-\theta) \quad (36)$$

The trigonometric changes to  $\tau_{mg}$  result in the equation for angular acceleration shown in Equation (37). Note that now both torque due to jet force and weight both act in the positive direction.

$$\alpha_3 = \frac{\tau_{F_n} + \tau_{mg}}{I_o} = \frac{\rho av^2 X \sin(\theta'_v) + mg O A \sin(-\theta)}{I_o} \quad (37)$$

As done in the previous two sections, evaluating integrals result in equations for angular velocity and time as shown in Equations (40) and (41) respectively.

$$\int_{\theta_i}^{\theta} \frac{\rho av^2 X \sin(\theta'_v) + mg O A \sin(-\theta)}{I_o} d\theta = \int_{\omega_i}^{\omega} \omega d\omega \quad (38)$$

$$\left[ \frac{\rho av^2 X \sin(\theta'_v) \theta + mg O A \cos(-\theta)}{I_o} \right]_{\theta_i}^{\theta} = \left[ \frac{\omega^2}{2} \right]_{\omega_i}^{\omega} \quad (39)$$

$$\omega_3 = \left( \frac{2((\rho av^2 X \sin(\theta'_v) \theta + mg O A \cos(-\theta)) - (\rho av^2 X \sin(\theta'_v) \theta_i + mg O A \cos(-\theta_i)))}{I_o} + \omega_i^2 \right)^{0.5} \quad (40)$$

$$t_3 = \int_{\theta_i}^{\theta} \frac{1}{\left( \frac{2((\rho av^2 X \sin(\theta'_v) \theta + mg O A \cos(-\theta)) - (\rho av^2 X \sin(\theta'_v) \theta_i + mg O A \cos(-\theta_i)))}{I_o} + \omega_i^2 \right)^{0.5}} d\theta + t_i \quad (41)$$

## B Moment of Inertia Calculations

In this section Equations for the gravity valve or waterwheel blade's moment of inertia will be derived based upon the chosen valve centre of mass,  $OA$ . The moment of inertia is dependent on the valves shape and weight distribution.  $OA$  is the distance to the valves centre of mass from pivot point  $O$ . The valve is assumed to be shaped as a uniform rectangular bar with added block weight which accounts for the chosen centre of mass as shown in Figure 29. Equations differ depending on whether the centre of mass, is less than, equal to or greater than  $\frac{L}{2}$ . If  $OA$  is equal to  $\frac{L}{2}$  no additional block weight is required. The added block weight is given a mass of  $M_1$  and the uniform bar has a mass of  $M_2$ . Both add to get valve weight,  $M$ . All that remains to be found is the ratio,  $r$ , of mass  $M_1 : M_2$ . The valves centre of mass,  $OA$  can be expressed in terms of the additional block weight mass ( $M_1$ ), distance from pivot to additional block weight centre of mass ( $d_1$ ), uniform bar mass ( $M_2$ ) and the distance from pivot to uniform bar centre of mass ( $d_2$ ) as shown in Equation (42). The  $M_1 : M_2$  ratio,  $r$  can be introduced to this equation which can then be rearranged to solve for  $r$ . This process is performed in Equation (43) and (44) when  $OA < \frac{L}{2}$  and Equations (45) and (46) when  $OA > \frac{L}{2}$ .

$$OA = \frac{d_1 M_1 + d_2 L M_2}{M} = \frac{d_1 M_1 r + d_2 L M_2 (1 - r)}{M} \quad (42)$$

Determining  $r$  when  $OA < \frac{L}{2}$ .

$$OA = \frac{0.5 O A M_1 + 0.5 L M_2}{M} = \frac{0.5 O A M r + 0.5 L M (1 - r)}{M} \quad (43)$$

$$r = \frac{OA - 0.5L}{0.5OA - 0.5L} \quad (44)$$

Determining  $r$  when  $OA > \frac{L}{2}$ .

$$OA = \frac{(OA + 0.5(L - OA))M_1 + 0.5LM_2}{M} = \frac{(OA + 0.5(L - OA))Mr + 0.5LM(1 - r)}{M} \quad (45)$$

$$r = \frac{OA - 0.5L}{OA + 0.5(L - OA) - 0.5L} \quad (46)$$

Once the weight distribution of the valve is known based on its centre of mass, the valve's moment of inertia can be calculated.

If  $OA < \frac{L}{2}$

$$I_o = \frac{1}{3} r m O A^2 + \frac{1}{3} (1 - r) m L^2 \quad (47)$$

If  $OA = \frac{L}{2}$

$$I_o = \frac{1}{3} m L^2 \quad (48)$$

If  $OA > \frac{L}{2}$

$$I_o = \frac{r m (L^3 - O A^3)}{3(L - O A)} + \frac{1}{3} (1 - r) m L^2 \quad (49)$$

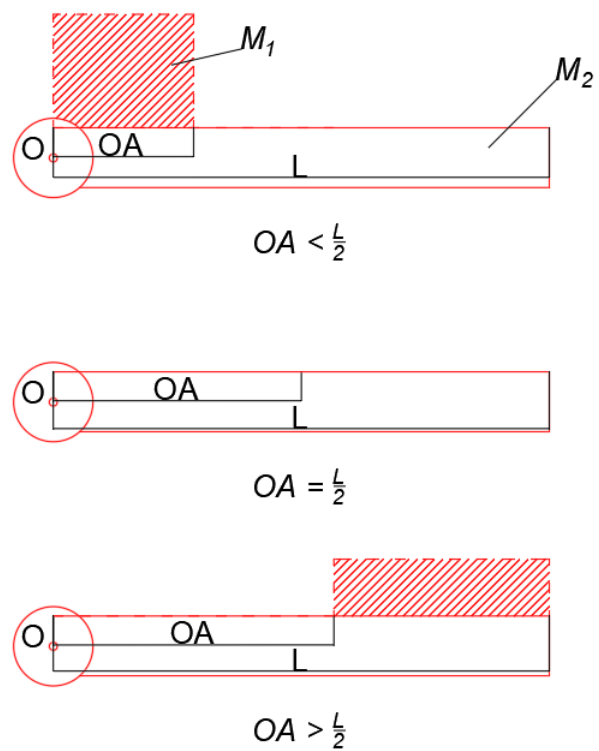


Figure 29: Three different configurations of valve or blade mass distribution depending on the chosen value of  $OA$ .

## C Waterwheel Theory Calculations

In this section detailed calculations used in the waterwheel theory are shown. The rotational angle during which the jet is blocked,  $\theta_j$  can be determined using trigonometry. The angle can be determined by adding two angles,  $\theta_{j1}$  and  $\theta_{j2}$  which can be calculated using the sine rule of the two triangles identified in Figure 30. Resulting Equations for  $\theta_{j1}$ ,  $\theta_{j2}$  and  $\theta_j$  are shown in Equations (50), (51) and (52) respectively. As  $\sin(\theta'_v)$  is equal to  $\sin(\pi - \theta'_v)$ , the equation for  $\theta_j$  can be simplified as shown in Equation (53). The Equation for  $\theta'_v$  remains the same as that with the gravity valve as shown in Equation (54).

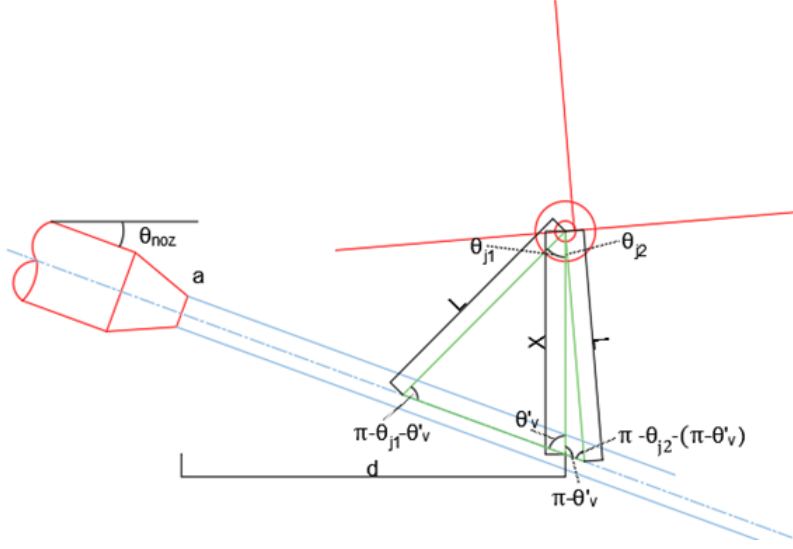


Figure 30: Trigonometric relations used to calculate the angle during which the jet stream is blocked by the waterwheel,  $\theta_j$

$$\theta_{j1} = \pi - \theta'_v - \sin^{-1}\left(\frac{X \sin(\theta'_v)}{L}\right) \quad (50)$$

$$\theta_{j2} = \theta'_v - \sin^{-1}\left(\frac{X \sin(\pi - \theta'_v)}{L}\right) \quad (51)$$

$$\theta_j = \pi - \sin^{-1}\left(\frac{X \sin(\theta'_v)}{L}\right) - \sin^{-1}\left(\frac{X \sin(\pi - \theta'_v)}{L}\right) \quad (52)$$

$$\theta_j = \pi - 2\sin^{-1}\left(\frac{X \sin(\theta'_v)}{L}\right) \quad (53)$$

$$\theta'_v = \frac{\pi}{2} - \theta_{noz} \quad (54)$$

The Equation for  $\theta'$  can now be determined. Unlike the gravity valve where  $\theta = 0$  is chosen as the position when the valve was vertical, the waterwheel's  $\theta = 0$  position is chosen as when the blade first touches the water stream. This results in an Equation for  $\theta'$  shown in Equation (55).

$$\theta' = \theta_{j1} - \theta + \theta'_v \quad (55)$$

### C.1 Method 1: Jet Velocity Assumption

Firstly vector jet stream velocity perpendicular to the blade ( $v$ ) must be converted to angular velocity ( $\omega$ ). This can be done using Equation (56) where  $r$  is the radius.

$$v = r\omega \quad (56)$$

In this system  $r$  is represented as  $OB$  as done in the gravity valve theory. If  $v$  and  $OB$  can be known throughout the period that the waterwheel blade is in contact with the jet, an average value for angular velocity can be determined which can then be used to determine system cycle time. Three phases are defined as shown in Figure 31. In each of these three phases Equations for  $v$  and  $OB$  change due to trigonometric relations. An overview of  $v$  and  $OB$  Equations as well as the theta boundaries of each phase is shown in Table 8. The vector jet velocity perpendicular to the blade,  $v$  is determined by taking the sine component of the jet velocity at the nozzle. The water jet is assumed to gain no velocity due to gravitational potential energy, any velocity gained is likely to be negligible due to small  $d$  values and high  $v$  values. Equations for  $OB$  are determined using the sine rule.

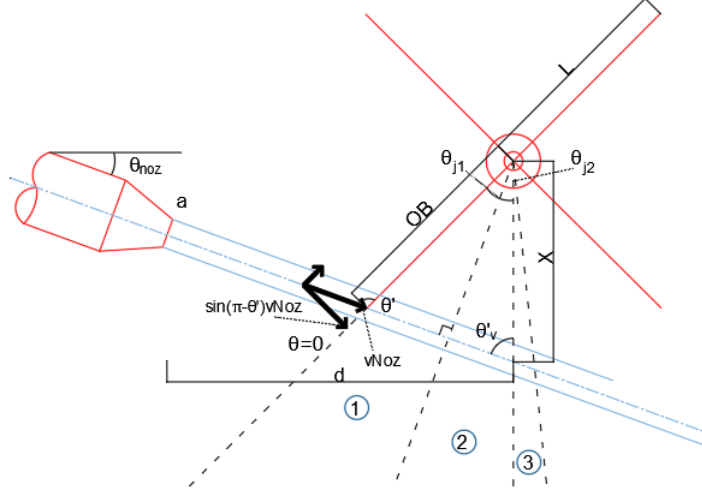


Figure 31: The three phases defined as a waterwheel blade blocks the jet stream.

Table 8: Overview of  $v$  and  $OB$  values as well as theta boundaries for each of the three defined waterwheel jet contact phases.

Phase	$v$	$OB$	$\theta$ boundaries
1	$\sin(\pi - \theta')v_{noz}$	$\frac{X \sin(\theta'_v)}{\sin(\pi - \theta')}$	0 to $(\theta_{j1} + \theta'_v - \frac{\pi}{2})$
2	$\sin(\theta')v_{noz}$	$\frac{X \sin(\theta'_v)}{\sin(\pi - \theta')}$	$(\theta_{j1} + \theta'_v - \frac{\pi}{2})$ to $\theta_{j1}$
3	$\sin(\theta')v_{noz}$	$\frac{X \sin(\pi - \theta'_v)}{\sin(\theta')}$	$\theta_{j1}$ to $\theta_j$

As it turns out  $\sin(\pi - x)$  is equal to  $\sin(x)$ . Therefore Equations for angular velocity are the same throughout all three phases. The Equation for angular velocity with respect to  $\theta$  is shown in Equation (57). Average angular velocity throughout the movement can be determined integrating Equation (57) over the theta boundary  $0 - \theta_j$  and dividing by  $\theta_j$  as shown in Equation (58). This average angular velocity value in rad/s can be converted to revolutions per second to determine cycle time as shown in Equation (59).

$$\omega = \frac{v}{r} = \frac{\sin(\theta')v_{noz}}{\frac{X \sin(\theta'_v)}{\sin(\theta')}} = \frac{\sin(\theta_{j1} - \theta + \theta'_v)v_{noz}}{\frac{X \sin(\theta'_v)}{\sin(\theta_{j1} - \theta + \theta'_v)}} \quad (57)$$

$$\omega_{avg} = \frac{1}{\theta_j} \left( \int_0^{\theta_j} \frac{\sin(\theta_{j1} - \theta + \theta'_v)v_{noz}}{\frac{X \sin(\theta'_v)}{\sin(\theta_{j1} - \theta + \theta'_v)}} d\theta \right) \quad (58)$$

$$\text{cycle time}_{m1} = \frac{1}{0.159155\omega_{avg}} \quad (59)$$

As the jet velocity method assumes a waterwheel spinning at constant angular velocity the jet open : close ratio can be determined using the angle during which the jet is blocked,  $\theta_j$  and the angle during which the jet is open. The angle in which the jet is open can be determined by subtracting  $\theta_j$  from the angle between the blades which is equal to  $\frac{2\pi}{n}$ . Therefore the jet open : close ratio can be determined as shown in Equation (60).

$$\text{open:close}_{m1} = \frac{\frac{2\pi}{n} - \theta_j}{\theta_j} \quad (60)$$

## C.2 Method 2: Force Considerations

When taking an approach that considers the forces acting on the waterwheel, instantaneous angular acceleration can be determined as done for the gravity valve system by using the angular form of Newton's second law shown in Equation (16). To apply this Equation the wheels moment of inertia ( $I_o$ ) and torque due to water force ( $\tau_{F_n}$ ) must be known. There is no torque due to blade weight for two, three and four bladed wheels as for every value of theta, the torque equates to zero as blades act in both positive and negative directions at the same magnitude.

The waterwheels moment of inertia can simply be determined by multiply  $I_o$  of each identical blade by the number of blades in each wheel. Torque due to water force can be determined by multiplying the force acting perpendicular to the blade ( $F_n$ ) by the distance from the waterwheel pivot to the water force ( $OB$ ). To do this the same issue occurs as outlined in Figure 31 where three phases within the jet impact boundary are identified to have differing  $F_n$  and  $OB$  Equations due to trigonometric changes. The values of  $F_n$ ,  $OB$  and resulting  $\tau_{F_n}$  values for each phase are outlined in Table 9.

Table 9: Overview of  $\tau_{F_n}$  values as well as  $\theta$  boundaries for each of the three defined waterwheel jet contact phases.

Phase	$F_n$	$OB$	$\tau_{F_n}$	$\theta$ boundaries
1	$\rho av^2 \sin(\pi - \theta')$	$\frac{X \sin(\theta'_v)}{\sin(\pi - \theta')}$	$\rho av^2 X \sin(\theta'_v)$	0 to $(\theta_{j1} + \theta'_v - \frac{\pi}{2})$
2	$\rho av^2 \sin(\theta')$	$\frac{X \sin(\theta'_v)}{\sin(\pi - \theta')}$	$\rho av^2 X \sin(\theta'_v)$	$(\theta_{j1} + \theta'_v - \frac{\pi}{2})$ to $\theta_{j1}$
3	$\rho av^2 \sin(\theta')$	$\frac{X \sin(\pi - \theta'_v)}{\sin(\theta')}$	$\rho av^2 X \sin(\pi - \theta'_v)$	$\theta_{j1}$ to $\theta_j$

It turns out the Equation for  $\tau_{F_n}$  is the same for all three phases as  $\sin(\theta') = \sin(\pi - \theta')$ , its magnitude is not dependent on the value of  $\theta$ . Using Equation 17, instantaneous angular acceleration can be determined when the jet impacts wheel blades as shown in Equation 61.

$$\alpha_{ww} = \frac{\tau_{F_n}}{I_o} = \frac{\rho av^2 X \sin(\theta'_v)}{I_o} \quad (61)$$

Next using the relationship shown in Equation (18), the expression for angular velocity with respect to theta can be found by solving the integral shown in Equation (62). The evaluated integral is shown in Equation (64).

$$\int_{\theta_i}^{\theta} \frac{\rho av^2 X \sin(\theta'_v)}{I_o} d\theta = \int_{\omega_i}^{\omega} \omega d\omega \quad (62)$$

$$\left[ \frac{\rho av^2 X \sin(\theta'_v) \theta}{I_o} \right]_{\theta_i}^{\theta} = \left[ \frac{\omega^2}{2} \right]_{\omega_i}^{\omega} \quad (63)$$

$$\omega_{ww} = \left( \frac{2((\rho av^2 X \sin(\theta'_v) \theta) - (\rho av^2 X \sin(\theta'_v) \theta_i))}{I_o} + \omega_i^2 \right)^{0.5} \quad (64)$$

Using the relationship in Equation (21), the expression for time can be found by evaluating the integral shown in Equation (65).

$$\int_{\theta_i}^{\theta} \frac{1}{\omega} d\theta = \int_{t_i}^t dt \quad (65)$$

$$t_{ww} = \int_{\theta_i}^{\theta} \frac{1}{\left( \frac{2((\rho av^2 X \sin(\theta'_v)\theta) - (\rho av^2 X \sin(\theta'_v)\theta_i))}{I_o} + \omega_i^2 \right)^{0.5}} d\theta + t_i \quad (66)$$

By applying the current Equations the waterwheel will accelerate whenever a waterwheel blade comes into contact with the jet. It will unrealistically gain and never lose angular velocity and would therefore never reach a constant optimal angular velocity. To solve this issue it is assumed the waterwheel velocity decreases when not in contact with the jet. This helps account for energy losses. The extent of this velocity decrease is calibrated to fit empirical data gathered from the physical experiment. The velocity when not in contact with the jet is chosen as the final velocity when in contact with the jet reduced by a constant calibrated scale factor.

System cycle time and jet open : close ratio for each revolution can be determined by using the derived equations to plot waterwheel motion over time. This is elaborated upon further in Section 3.2 where the waterwheel's analytical model is explained.

## D Gravity Valve Matlab Script

Shown below is the MATLAB script used to model the gravity driven pivot valve concept.

```
1 %Modelling Gravity Valve Concept
2 %Exitflag = 0: System satisfies all requirements.
3 %Exitflag = 1: Valve exceeds negative boundary.
4 %Exitflag = 2: Insufficient force to leave stream.
5 %Exitflag = 3: Insufficient valve open:close ratio.
6 clear, clc
7
8 %Input Variables
9 Theta_Noz = 20; %Nozzle angle to horizontal in degrees.
10 L = 0.15; %Valve length in metres
11 m = 0.224; %Valve mass in kg.
12 X = 0.072; %Vertical distance from pivot to jet impact in metres.
13 a = 0.00007854; %Area of jet stream in metres squared (circle w/ diameter 0.5cm)
14 v_Noiz = 2.55; %Velocity of jet stream in metres per second.
15 d = 0.25; %Horizontal distance from the jet nozzle to vertical valve in metres.
16 OA = 0.075; %Distance along valve to centre of mass in metres.
17 rho = 1000; %Density of water in kilograms per metre cubed.
18 g = 9.81; %Accerlaration due to gravity in metres per second squared.
19 Theta_f = pi/2; %Angle in which valve starts at
20 smoothness = 0.001; %Interval in which theta is increased by each step.
21 maxcycle = 2; %Chosen number of swing cycles to model.
22
23 %Resulting parameters
24 %Calculate impact angle between jet and vertical valve.
25 Theta_Impact_v = pi/2 - (Theta_Noz*(pi/180));
26
27 if OA < L/2
28 %Calculate ratio of additional block weight:bar weight
29 r = ((OA - 0.5*L)/(0.5*OA - 0.5*L));
30 %Moment of inertia for rectangular rod with additional weight on half closer to pivot.
31 Io = 1/3*r*m*OA^2 + 1/3*(1-r)*m*L^2;
32 elseif OA == L/2
33 Io = 1/3*m*L^2; %Moment of inertia for rectangular rod around pivot point.
34 elseif OA > L/2 && OA < L
35 %Calculate ratio of additional block weight:bar weight
36 r = ((0.5*L - (L-OA))/(0.5*L - 0.5*(L-OA)));
37 %Moment of inertia for rectangular rod with additional weight half further from pivot.
38 Io = ((r*m)/(L-OA))*((L^3)/3 - (OA^3)/3) + 1/3*(1-r)*m*L^2;
39 else
40 disp('Error, OA must be less than L')
41 end
42
43 %Calculate positive theta boundary: angle when valve no longer
44 %touches the jet stream in positive theta.
45 Theta_bpos = Theta_Impact_v - asin((X*sin(pi-Theta_Impact_v))/L);
46 %Calculate negative theta boundary: angle in which the valve no longer
47 %touches the jet stream in negative theta.
48 Theta_bneg = -1*(pi - Theta_Impact_v - asin((X*sin(Theta_Impact_v))/L));
49
50 %Specify anonymous functions derived from theory used throughout model
51 %Torque due to jet as function of theta.
52 T_Fn = @(Theta) rho*a*v^2*sin(Theta_Impact_v - ...
53 Theta)*(X*sin(pi-Theta_Impact_v))/(sin(Theta_Impact_v - Theta));
54 %Torque due to weight as function of theta.
55 T_mg = @(Theta) m*g*OA*sin(Theta);
56 %Impact velocity at valve impact using bernoulli as function of theta.
57 vfunction = @(Theta) (v_Noiz.^2+2.*9.81.*(tan(Theta_Noz.*(pi/180)).*d + ...
58 cos(Theta).*(sin(pi/2-Theta_Impact_v)*tan(Theta).*X)./sin(Theta_Impact_v - ...
59 Theta))).^0.5;
```

```

59 %Angular acceleration as function of theta when jet and weight force are acting.
60 alpha_Fnmng = @(Theta) (rho*a*(v_NoZ.^2)*X*sin(pi-Theta_Impact_v)-(m*g*OA*sin(Theta)))/Io;
61 %Angular acceleration as function of theta when only force when only weight force acts.
62 alpha_mg = @(Theta) (-1*m*g*OA*sin(Theta))/Io;
63
64 alpha_Fnmgminus = @(Theta) ...
    (rho*a*(v_NoZ.^2).*X*sin(Theta_Impact_v)+m*g*OA*sin(-1.*Theta))/Io;
65
66 %Angular velocity as function of theta when jet and weight force are acting.
67 omega_Fnmng = @(Theta,Theta_i,Omega_i) ...
    ((2.*(rho*a*(v_NoZ.^2).*X.*sin(pi-Theta_Impact_v).*Theta+m.*g.*OA.*cos(Theta))-...
68    (rho.*a.*(v_NoZ.^2).*X.*sin(Theta_Impact_v).*Theta_i+m.*g.*OA.*...
69    cos(Theta_i)))/Io)+Omega_i.^2).^0.5;
70 %Angular velocity as function of theta when only weight force is acting.
71 omega_mg = @(Theta,Theta_i,Omega_i) ...
    ((2.*(m.*g.*OA.*cos(Theta)-m.*g.*OA.*cos(Theta_i)))/Io)+(Omega_i.^2).^0.5;
72 %Angular velocity as function of theta when jet & weight force act & when theta is ...
    negative.
73 omega_Fnmgminus = @(Theta,Theta_i,Omega_i) ...
    ((2.*(rho*a*(v_NoZ.^2).*X.*sin(Theta_Impact_v).*Theta+m.*g.*OA.*cos(-1.*Theta))-...
74    (rho.*a.*(v_NoZ.^2).*X.*sin(Theta_Impact_v).*Theta_i+m.*g.*OA.*...
75    cos(-1.*Theta_i)))/Io)+Omega_i.^2).^0.5;
76
77 %1/angular velocity: integrated to get time as function of theta when jet and weight ...
    force are acting.
78 t_Fnmng = @(Theta,Theta_i,Omega_i) ...
    1./(((2.*(rho*a*(v_NoZ.^2).*X.*sin(pi-Theta_Impact_v).*Theta+m.*g.*OA.*cos(Theta))-...
79    (rho.*a.*(v_NoZ.^2).*X.*sin(pi-Theta_Impact_v).*Theta_i+m.*g.*OA.*...
80    cos(Theta_i)))/Io)+Omega_i.^2).^0.5;
81 %1/angular velocity: integrated to get time as a function of theta when only weight ...
    force is acting.
82 t_mg = @(Theta,Theta_i,Omega_i) ...
    1./(((2.*(m.*g.*OA.*cos(Theta)-m.*g.*OA.*cos(Theta_i)))/Io)+(Omega_i.^2).^0.5;
83 %1/angular velocity: integrated to get time as a function of theta when jet & weight ...
    force act & when theta is negative.
84 t_Fnmgminus = @(Theta,Theta_i,Omega_i) ...
    1./(((2.*(rho*a*(v_NoZ.^2).*X.*sin(Theta_Impact_v).*Theta+m.*g.*OA.*cos(-1.*Theta))-...
85    (rho.*a.*(v_NoZ.^2).*X.*sin(Theta_Impact_v).*Theta_i+m.*g.*OA.*...
86    cos(-1.*Theta_i)))/Io)+Omega_i.^2).^0.5;
87
88
89 %Initiate starting values:
90 omega = 0;           %Angular velocity is initially 0.
91 alpha = 0;          %Angular acceleration is initially 0.
92 t = 0;              %Time is initially 0.
93 i = 1;              %Cycle number is initially 1.
94 Counter = 1;        %Counter for tracking data is initially 1.
95 exitflag = 0;       %Exitflag status initially 0.
96
97 %Theta_i is the starting boundary theta value for each swing section and
98 %Theta_f is the final boundary value for a given swing section.
99
100 %Model the system whilst no exitflags and whilst chosen number of cycles are not yet ...
    modelled.
101 while exitflag ==0 && i ≤ maxcycle
102
103 %% Swing cycle 1-2 (-ve direction)
104 %Initiate values
105 Theta_i = Theta_f;
106 Omega_i = omega;
107 Theta_f = Theta_bpos;
108 t_i = t;
109 %Calculate swing position 1-2
110 %For loop of theta values to be tested: spaced at intervals equal to smoothness ...
    between boundaries theta_i and theta_f

```

```

111 for Theta = ...
    linspace(Theta_i-smoothness,Theta_f,round(abs((Theta_f-(Theta_i-smoothness)))/smoothness))
112 thetadata(Counter) = Theta; %Record theta data
113 v = 0; %Impact velocity is taken as 0 as valve is not in contact ...
    with stream in this swing cycle
114 vdata(Counter) = v; %Record impact velocity data
115 alpha = alpha_mg(Theta); %Use function to calculate angular acceleration at this ...
    theta value
116 alphadata(Counter) = alpha; %Record angular velocity data
117
118 omega = -1.*omega_mg(Theta,Theta_i,Omega_i); %Use function to calculate angular ...
    velocity at this theta value, it is multiplied by -1 as valve travels negative ...
    direction (same as negative integral flipping boundaries)
119 omegadata(Counter)=omega; %Record angular velocity data.
120
121 t = -1.*integral(@(Theta)t_mg(Theta,Theta_i,Omega_i),Theta_i,Theta) +t_i; %Use ...
    integral tool to integrate t function and find t for this theta value.
122 tdata(Counter) = t; %Record t data
123 Counter = Counter+1; %Add counter for next data point.
124 end
125
126 %% Swing cycle 2-3 (-ve direction)
127 %Initiate values
128 Theta_i = Theta_f;
129 Omega_i = omega;
130 %Determine the max value of theta that can be reached on the downswing.
131 syms x
132 eqn = ((2.*(rho.*a.*(v_NoZ.^2).*X.*sin(pi-Theta_Impact_v).*x+m.*g.*OA.*cos(x))-...
133     (rho.*a.*(v_NoZ.^2).*X.*sin(pi-Theta_Impact_v).*Theta_i+m.*g.*OA.*...
134     cos(Theta_i)))./Io)+Omega_i.^2).^0.5 == 0;
135 Theta_f = vpsolve(eqn,x,[Theta_bpos;0]);
136 Theta_f = double(Theta_f);
137 %If the equation has no real answer the theta value is negative, therefore
138 %section 2-3 finishes as theta_f = 0
139 if isempty(Theta_f) == 1
140     Theta_f = 0;
141 end
142 t_i = t;
143 %Calculate swing position 2-3
144 for Theta = ...
    linspace(Theta_i-smoothness,Theta_f,round(abs((Theta_f-(Theta_i-smoothness)))/smoothness))
145 thetadata(Counter) = Theta;
146 v = vfunction(Theta);
147 vdata(Counter) = v;
148 alpha = alpha_Fnmg(Theta);
149 alphadata(Counter) = alpha;
150
151 omega = -1.*omega_Fnmg(Theta,Theta_i,Omega_i);
152 if omega == 0
153     omega = 1e-20; %avoid 0 omega values to enable t integration (cant do 1/0).
154 end
155 omegadata(Counter)=omega;
156
157 t = -1.*integral(@(Theta)t_Fnmg(Theta,Theta_i,Omega_i),Theta_i,Theta) +t_i;
158 tdata(Counter) = t;
159 Counter = Counter+1;
160 end
161
162 %Only calculate phase 3 (negative theta) if theta_f from previous step is
163 %equal to 0
164 if Theta_f == 0
165 %% Swing cycle 3-4 (-ve direction)
166 %Initiate values
167 Theta_i = Theta_f;
168 Omega_i = omega;
169 %Calculate the max negative angle the valve reaches by solving omega =0.

```

```

170 syms x
171 eqn = ((2.*(rho.*a.*(v_NoZ.^2).*X.*sin(Theta_Impact_v).*x+m.*g.*OA.*cos(-x))-...
172     (rho.*a.*(v_NoZ.^2).*X.*sin(Theta_Impact_v).*Theta_i+m.*g.*OA.*...
173     cos(-Theta_i)))/Io)+Omega_i.^2).^0.5 == 0;
174 Theta_f = vpasolve(eqn,x,[0;-pi/2]);
175 Theta_f = double(Theta_f);
176 %If the calculated theta_f exceeds the negative boundary show exitflag:1
177 if Theta_f < (Theta_bneg)
178     exitflag = 1;
179     disp('Valve exceeds negative boundary')
180 end
181 t_i = t;
182 %Calculate swing position 3-4
183 for Theta = ...
184     linspace(Theta_i-smoothness,Theta_f,round(abs((Theta_f-(Theta_i-smoothness)))/smoothness))
185 thetadata(Counter) = Theta;
186 v = vfunction(Theta);
187 vdata(Counter) = v;
188 alpha = alpha_Fnmgminus(Theta);
189 alphadata(Counter) = alpha;
190 omega = -1.*omega_Fnmgminus(Theta,Theta_i,Omega_i);
191 if omega == 0
192     omega = 1e-20; %avoid 0 omega values to enable t integration.
193 end
194 omegadata(Counter) = omega;
195
196 t = -1.*integral(@(Theta)t_Fnmgminus(Theta,Theta_i,Omega_i),Theta_i,Theta) +t_i;
197 tdata(Counter) = t;
198 Counter = Counter+1;
199 end
200
201 %% Swing cycle 4-5 (+ve direction)
202 %Initiate values
203 Theta_i = Theta_f;
204 Omega_i = omega;
205 Theta_f = 0;
206 t_i = t;
207 %Calculate swing position 4-5
208 for Theta = ...
209     linspace(Theta_i+smoothness,Theta_f,round(abs((Theta_f-(Theta_i+smoothness)))/smoothness))
210 thetadata(Counter) = Theta;
211 v = vfunction(Theta);
212 vdata(Counter) = v;
213 alpha = alpha_Fnmgminus(Theta);
214 alphadata(Counter) = alpha;
215
216 omega = omega_Fnmgminus(Theta,Theta_i,Omega_i);
217 omegadata(Counter) = omega;
218
219 t = integral(@(Theta)t_Fnmgminus(Theta,Theta_i,Omega_i),Theta_i,Theta) +t_i;
220 tdata(Counter) = t;
221 Counter = Counter+1;
222 end
223
224 %% Swing cycle 5-6 (+ve direction)
225 %Initiate values
226 Theta_i = Theta_f;
227 Omega_i = omega;
228 %Calculate whether there is a solution for omega equaling zero within phase
229 %2 in the jet stream, this indicates insufficient jet torque.
230 syms x
231 eqn = ((2.*(rho.*a.*(v_NoZ.^2).*X.*sin(pi-Theta_Impact_v).*x+m.*g.*OA.*cos(x))-...
232     (rho.*a.*(v_NoZ.^2).*X.*sin(pi-Theta_Impact_v).*Theta_i+m.*g.*OA.*...
233     cos(Theta_i)))/Io)+Omega_i.^2).^0.5 == 0;

```

```

234 Theta_f = vpasolve(eqn,x,[Theta_i+0.0001;Theta_bpos]);
235 Theta_f = double(Theta_f);
236 %If there is a solution display exitflag:2
237 if isempty(Theta_f) == 0
238     exitflag = 2;
239     disp('Force isnt sufficient to leave water stream')
240 else
241     %If there is not a solution theta_f is simply the positive theta
242     %boundary
243     Theta_f = Theta_bpos;
244 end
245 t_i = t;
246 %Calculate swing position 5-6
247 for Theta = linspace(Theta_i,Theta_f,round(abs((Theta_f-Theta_i))/smoothness))
248     thetadata(Counter) = Theta;
249     v = vfunction(Theta);
250     vdata(Counter) = v;
251     alpha = alpha_Fnmg(Theta);
252     alphadata(Counter) = alpha;
253
254     omega = omega_Fnmg(Theta,Theta_i,Omega_i);
255     if omega == 0
256         omega = 1e-20; %avoid 0 omega values to enable t integration.
257     end
258     omegadata(Counter)=omega;
259
260     t = integral(@(Theta)t_Fnmg(Theta,Theta_i,Omega_i),Theta_i,Theta) +t_i;
261     tdata(Counter) = t;
262     Counter = Counter+1;
263 end
264
265 if exitflag == 0
266     %% Swing cycle 6-1 (+ve direction)
267     %Initiate values
268     Theta_i = Theta_f;
269     Omega_i = omega;
270     %Solve omegal equation to determine angle valve swings back up to
271     Theta_f = acos(((-(Omega_i.^2)*Io)/(2.*m.*g.*OA))+cos(Theta_i));
272     t_i = t;
273     %Calculate swing position 6-1
274     for Theta = ...
275         linspace(Theta_i+smoothness,Theta_f,round(abs((Theta_f-(Theta_i+smoothness)))/smoothness))
276         thetadata(Counter) = Theta;
277         v = 0; %impact velocity is zero as valve isnt in contact with jet.
278         vdata(Counter) = v;
279         alpha = alpha_mg(Theta);
280         alphadata(Counter) = alpha;
281         omega = omega_mg(Theta,Theta_i,Omega_i);
282         if isreal(sqrt(omega)) == 0
283             omega = 1e-20; %made positive to avoid complex numbers and non zero for t ...
284                 integration.
285         end
286         omegadata(Counter)=omega;
287
288         t = integral(@(Theta)t_mg(Theta,Theta_i,Omega_i),Theta_i,Theta) +t_i;
289         tdata(Counter) = t;
290         Counter = Counter+1;
291     end
292 end
293 i = i+1; %increase i for next swing cycle
294 end
295
296 if exitflag == 0 || exitflag == 3

```

```

297 [~,idx] = mink(abs(thetadata-Theta_bpos),maxcycle*2); %Find counter points at ...
    positive theta boundary.
298 cycletime = tdata((Counter-1)/maxcycle); %Calculate systems cycle time as simulation ...
    time/number of cycles.
299 opentime = tdata(idx(1)).*2; %Calculate open time as two times time taken to reach ...
    first positive theta boundary.
300 closetime = tdata(idx(2))-tdata(idx(1)); %Calculate close time as time between first ...
    and second theta positive boundary.
301 ratio = opentime./closetime;
302 if ratio > 19 || ratio < 4 %If calculated open:close ratio doesnt meet Deltares ...
    requirements exitflag = 3.
303     exitflag = 3;
304 end
305 %Table giving system performance overview.
306 T = table([exitflag;cycletime;opentime;closetime;ratio],...
307     'VariableNames',{'Values'},...
308     'RowNames',{'Exitflag' 'Cycletime' 'Opentime' 'Closetime' 'OpenCloseRatio'});
309 disp(T)
310 else %If exitflag 1 or 2 performance overview cannot be given.
311     [~,idx] = mink(abs(thetadata-Theta_bpos),2); %Find counter points at positive ...
        theta boundary
312 end
313
314 %Display graph of impact velocity over time.
315 figure(1) , clf(1) , hold on
316 plot(tdata,vdata,'k-','LineWidth',3)
317 for i = 1:length(idx)
318     if rem(i, 2) == 0
319         Lv = ...
            plot(tdata(idx(i)),vdata(idx(i)),'o','MarkerEdgeColor','k','MarkerFaceColor','r');
320     else
321         Etr = ...
            plot(tdata(idx(i)),vdata(idx(i)),'o','MarkerEdgeColor','m','MarkerFaceColor','c');
322     end
323 end
324 title('Variation of jet velocity on impact over time')
325 legend([Etr Lv],'Enter Stream','Leave Stream')
326 ylabel('Velocity (ms-1)')
327 xlabel('Time (s)')
328 %Display graph of valve angle over time.
329 figure(2) , clf(2) , hold on
330 plot(tdata,thetadata,'k-','LineWidth',3)
331 for i = 1:length(idx)
332     if rem(i, 2) == 0
333         Lv = ...
            plot(tdata(idx(i)),thetadata(idx(i)),'o','MarkerEdgeColor','k','MarkerFaceColor','r');
334     else
335         Etr = ...
            plot(tdata(idx(i)),thetadata(idx(i)),'o','MarkerEdgeColor','m','MarkerFaceColor','c');
336     end
337 end
338 title('Variation of theta over time')
339 legend([Etr Lv],'Enter Stream','Leave Stream')
340 ylabel('Theta (rad)')
341 xlabel('Time (s)')
342 %Display graph of angular velocity over time.
343 figure(3) , clf(3) , hold on
344 plot(tdata,omegadata,'k-','LineWidth',3)
345 for i = 1:length(idx)
346     if rem(i, 2) == 0
347         Lv = ...
            plot(tdata(idx(i)),omegadata(idx(i)),'o','MarkerEdgeColor','k','MarkerFaceColor','r');
348     else
349         Etr = ...
            plot(tdata(idx(i)),omegadata(idx(i)),'o','MarkerEdgeColor','m','MarkerFaceColor','c');
350     end
351 end

```

```

351 end
352 title('Variation of angular velocity over time')
353 legend([Etr Lv], 'Enter Stream', 'Leave Stream')
354 ylabel('Angular velocity (ms-1)')
355 xlabel('Time (s)')
356 %Display graph of angular acceleration over time.
357 figure(4) , clf(4) , hold on
358 plot(tdata,alphadata,'k-', 'LineWidth',3)
359 for i = 1:length(idx)
360     if rem(i, 2) == 0
361         Lv = ...
362             plot(tdata(idx(i)),alphadata(idx(i)), 'o', 'MarkerEdgeColor', 'k', 'MarkerFaceColor', 'r');
363     else
364         Etr = ...
365             plot(tdata(idx(i)),alphadata(idx(i)), 'o', 'MarkerEdgeColor', 'm', 'MarkerFaceColor', 'c');
366     end
367 end
368 title('Variation of angular acceleration over time')
369 legend([Etr Lv], 'Enter Stream', 'Leave Stream')
370 ylabel('Angular acceleration (ms-2)')
371 xlabel('Time (s)')

```

## E Waterwheel Matlab Script

Shown below is the MATLAB script used to model the waterwheel concept.

```
1 %Modelling waterwheel concept
2 clear, clc
3
4 %Input Variables
5 Theta_Noz = 20; %Nozzle angle to horizontal in degrees.
6 L = 0.15; %Blade length in metres
7 m = 0.0485; %Blade mass in kg.
8 n = 2; %Number of blades
9 X = 0.097; %Vertical distance from pivot to jet impact in metres when blade ...
    is vertical.
10 a = 0.00007854; %Area of jet stream in metres squared (circle w/ diameter 0.5cm)
11 v_Noiz = 2.55; %Velocity of jet stream in metres per second.
12 d = 0.25; %Horizontal distance from the jet nozzle to vertical valve in metres.
13 OA = 0.075; %Distance along blade to centre of mass in metres.
14 rho = 1000; %Density of water in kilograms per metre cubed.
15 g = 9.81; %Accerlaration due to gravity in metres per second squared.
16 smoothness = 0.01; %Interval in which theta is increased by each step.
17 maxcycle = 12; %Number of revolutions modelled using method 2 - force ...
    considerations.
18 njofactor = 0.925; %No jet omega factor - scale factor for angular velocity when
19 %jet is not in contact with blades (must be less than 1 -slower when not in contact)
20
21 %Resulting parameters
22 %Calculate impact angle between jet and vertical blade.
23 Theta_Impact_v = pi/2 - (Theta_Noz*(pi/180));
24
25 %Calculate moment of inertia based on blade centre of mass (OA)
26 if OA < L/2
27 %Calculate ratio of additional block weight:bar weight
28 r = ((OA -0.5*L)/(0.5*OA-0.5*L));
29 %Moment of inertia for rectangular rod with additional weight on half closer to pivot.
30 Io = 1/3*r*m*OA^2 + 1/3*(1-r)*m*L^2;
31 elseif OA == L/2
32 Io = 1/3*m*L^2; %Moment of inertia for rectangular rod around pivot point.
33 elseif OA > L/2 && OA < L
34 %Calculate ratio of additional block weight:bar weight
35 r = ((0.5*L-(L-OA))/(0.5*L-0.5*(L-OA)));
36 %Moment of inertia for rectangular rod with additional weight half further from pivot.
37 Io = ((r*m)/(L-OA))*((L^3)/3-(OA^3)/3) + 1/3*(1-r)*m*L^2;
38 else
39 disp('Error, OA must be less than L')
40 end
41
42 %Moment of inertia for entire wheel is equal to summation of all blade moment
43 %of inertias.
44 Io = Io.*n;
45
46 %Calculate theta angle for which valve is within jet
47 Theta_j1 = pi - Theta_Impact_v - asin((X*sin(Theta_Impact_v))/L);
48 Theta_j2 = Theta_Impact_v - asin((X*sin(pi-Theta_Impact_v))/L);
49 Theta_j = pi - asin((X*sin(Theta_Impact_v))/L) - asin((X*sin(pi-Theta_Impact_v))/L);
50
51 %% Method 1: Wheel velocity = jet velocity
52 %Function for angular velocity (v/r)
53 omegaangular = @(Theta) (sin(Theta_j1-Theta+Theta_Impact_v)*v_Noiz)./...
54 ((X*sin(Theta_Impact_v))./(sin(Theta_j1-Theta+Theta_Impact_v)));
55
56 %Average velocity during jet impact equal to integral of omega between 0 -
57 %theta-j multiplied by 1/Theta-j
58 omavg = (1/(Theta_j))*integral(@(Theta)omegaangular(Theta),0,Theta_j);
59 %Convert angular velocity to revolutions per second
```

```

60 revpersec = 0.159155*omavg;
61 %Calculate cycle time for method 1
62 cycletimejetvelmodel = 1/revpersec;
63 %Calculate jet open:close ratio
64 ratiojetvelmodel = ((2.*pi/n)-Theta_j)/Theta_j;
65
66 %% Method 2: Force Considerations
67 %Define anonymous functions
68 %Angular acceleration as function of theta due to jet force
69 alpha_p123 = @(Theta) (rho*a*(v.Noz.^2)*X*sin(Theta_Impact_v))/Io;
70 %Angular velocity as function of theta due to jet force
71 omega_p123 = @(Theta,Theta_i,Omega_i) ...
    ((2.*((rho*a*(v.Noz.^2).*X.*sin(pi-Theta_Impact_v).*Theta ...
    -(rho.*a*(v.Noz.^2).*X.*sin(pi-Theta_Impact_v).*Theta_i)))/Io)+Omega_i.^2).^0.5;
72 %1/angular velocity: integrated to get time as a function of theta
73 time_p123 = @(Theta,Theta_i,Omega_i) ...
    1./(((2.*((rho*a*(v.Noz.^2).*X.*sin(pi-Theta_Impact_v).*Theta ...
    -(rho.*a*(v.Noz.^2).*X.*sin(pi-Theta_Impact_v).*Theta_i)))/Io)+Omega_i.^2).^0.5;
74
75 %Initial values
76 omega = 0; %Waterwheel angular velocity is initially 0
77 t = 0; %Time starts at 0
78 i = 1; %Start on revolution number 1
79 Counter = 1; %Data counter starts at 1
80 t_jetclose = zeros(1,maxcycle); %Jet close time as zero vector
81 t_jetopen = zeros(1,maxcycle); %Jet open time as zero vector
82
83 %Keep repeating process until desired number of revolutions is modelled
84 while i <= maxcycle
85     Theta_rev = 0;
86     %Keep repeating until number of blades on wheel are modelled
87     for ii = 1:n
88         %% Jet contact phase
89         %Initiate values
90         Theta_i = 0; %Starting value of theta is zero
91         Omega_i = omega; %Starting value of omega equal to current omega
92         Theta_f = Theta_j; %End value theta equal to Theta_j
93         t_i = t;
94
95         %For loop of theta values to be tested: spaced at intervals equal to smoothness ...
96         %between boundaries theta_i and theta_f
97         for Theta = ...
98             linspace(Theta_i,Theta_f,round(abs((Theta_f-(Theta_i-smoothness)))/smoothness))
99             thetadata(Counter) = Theta+Theta_rev; %Record theta data, theta_n added depending on ...
100             blade number
101             alpha = alpha_p123(Theta); %Use function to calculate angular acceleration at this ...
102             theta value
103             alphadata(Counter) = alpha; %Record angular acceleration data
104             omega = omega_p123(Theta,Theta_i,Omega_i); %Use function to calculate angular velocity
105             omegadata(Counter)=omega; %Record angular velocity data.
106             t = integral(@(Theta)time_p123(Theta,Theta_i,Omega_i),Theta_i,Theta) +t_i; %Use ...
107             integral tool to integrate t function and find t for this theta value.
108             tdata(Counter) = t; %Record t data
109             Counter = Counter+1; %Add counter for next data point.
110         end
111         t_jetclose(i) = t_jetclose(i) + (t-t_i); %Time jet is closed is equal to previous ...
112         blade jet close time plus this blades jet close time.
113
114         %% No jet contact phase
115         %Initiate values
116         Theta_i = Theta; %Starting value of theta equal to current theta
117         Omega_i = omega; %Starting value of omega equal to current omega
118         Theta_f = (2*pi)/n; %End value theta equal to angle between blades
119         t_i = t;

```

```

116 for Theta = ...
    linspace(Theta_i+smoothness,Theta_f,round(abs((Theta_f-(Theta_i-smoothness)))/smoothness))
117 thetadata(Counter) = Theta+Theta_rev; %Record theta data
118 alphadata(Counter) = 0; %Angular acceleration just taken as zero - doesnt affect results
119 %Omega when not in contact with jet is calibrated to decrease to 0.925 time
120 %omega_i
121 omega = njofactor.*Omega_i;
122 omegadata(Counter)=omega; %Record angular velocity data.
123
124 %t simply determined using t = angle/velocity due to constant velocity.
125 t = (Theta-Theta_i)./omega +t_i;
126 tdata(Counter) = t; %Record t data
127 Counter = Counter+1; %Add counter for next data point.
128 end
129 t_jetopen(i) = t_jetopen(i) + (t-t_i); %Time jet is open is equal to previous blade ...
    jet open time plus this blades jet open time.
130 Theta_rev = Theta;
131 end
132 %Open:close ratio and cycletime calculated for current revolution
133 ratiodata(i) = t_jetopen(i)./t_jetclose(i);
134 cycletimedata(i) = t_jetclose(i) + t_jetopen(i);
135 i = i+1; %Next revolution
136 end
137
138 %Output overview table
139 T = ...
    table([cycletimejetvelmodel;ratiojetvelmodel;cycletimedata(maxcycle);ratiodata(maxcycle)],...
140 'VariableNames',{'Values'},'RowNames',{'CycletimeJetModel' 'OpenCloseRatioJetModel' ...
    'CycletimeForcemodel' 'OpenCloseRatioForcemodel'});
141 disp(T)
142
143 %Display graph of revolution angle over time.
144 figure(1) , clf(1) , hold on
145 plot(tdata,thetadata,'k-','LineWidth',3)
146 title('Variation of theta over time')
147 ylabel('Theta (rad)')
148 xlabel('Time (s)')
149 %Display graph of wheel angular velocity over time.
150 figure(2) , clf(2) , hold on
151 plot(tdata,omegadata,'k-','LineWidth',3)
152 title('Variation of angular velocity over time')
153 ylabel('Angular velocity (ms^-1)')
154 xlabel('Time (s)')
155 %Display graph of wheel angular acceleration over time.
156 figure(3) , clf(3) , hold on
157 plot(tdata,alphadata,'k-','LineWidth',3)
158 title('Variation of angular acceleration over time')
159 ylabel('Angular acceleration (ms^-2)')
160 xlabel('Time (s)')
161 %Display graph of cycle time over revolutions.
162 figure(4) , clf(4) , hold on
163 plot(1:maxcycle,cycletimedata,'k-','LineWidth',3)
164 title('How cycletime changes depending on revolution number')
165 xlabel('Revolution number')
166 ylabel('Cycletime (s)')

```

## F Impression of the Tested Braking System

Shown below is an impression of the frictional braking system tested in the waterwheel experiments.

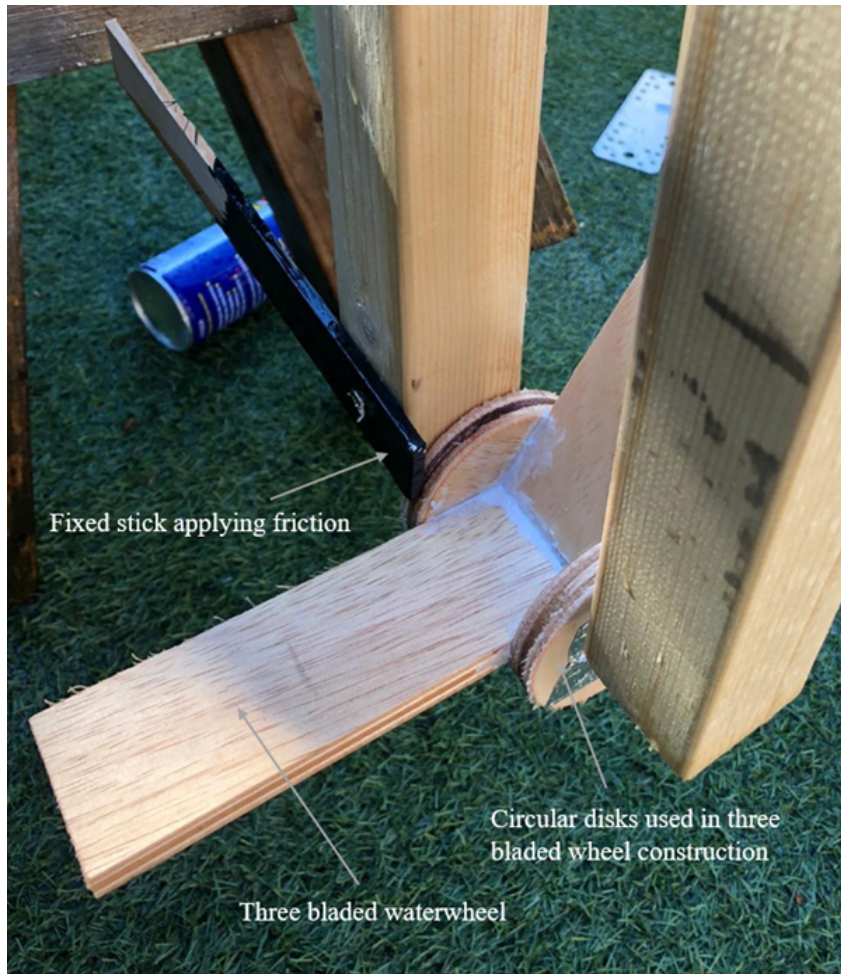


Figure 32: Impression of the waterwheel's tested frictional braking system.

## G Jet Impact Velocity Using Bernoulli

The jet stream velocity as it leaves the nozzle ( $v_{noz}$ ) is less than the velocity as it impacts the valve ( $v$ ) because gravitational potential energy is transferred to kinetic energy. Bernoulli's equation is used to estimate jet stream velocity as it impacts the valve. Taking the point where the jet stream leaves the nozzle as point 1 and point of jet stream impact with the valve as point 2, Bernoulli's equation can be used. The full Bernoulli's equation is shown in Equation 67 where  $P$  is pressure,  $\rho$  is density,  $v$  is velocity,  $g$  is acceleration due to gravity and  $h$  is vertical height with respect to a chosen datum.

$$P_1 + \frac{1}{2}\rho v_1^2 + \rho g h_1 = P_2 + \frac{1}{2}\rho v_2^2 + \rho g h_2 \quad (67)$$

At both points water is at atmospheric pressure, therefore pressure ( $P$ ) can be removed from both sides of the equation. Point two is taken as the datum thus  $h_2$  equals zero. This results in:

$$\frac{1}{2}\rho v_{noz}^2 + \rho g h_1 = \frac{1}{2}\rho v_2^2 \quad (68)$$

Density ( $\rho$ ) can be cancelled out and the equation can be rearranged to find water velocity at valve impact,  $v_2$ , as shown in Equation (69).

$$v_2 = (v_{noz}^2 + 2gh_1)^{0.5} \quad (69)$$

All that is left is to determine  $h_1$  as function of theta.

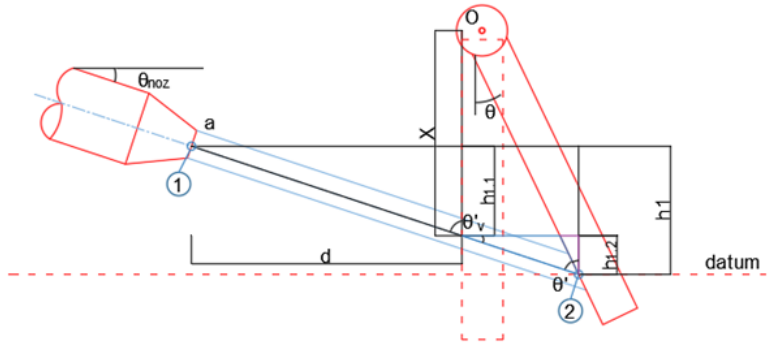


Figure 33: Trigonometric relations used to determine  $h_1$  as a function of theta to complete Bernoulli's equation.

From Figure 33,  $h_{1,1}$  and  $h_{1,2}$  can be determined using trigonometry.  $h_{1,1}$  is shown in Equation (70) and is determined from a simple right angled triangle using  $d$  and  $\theta_{noz}$ .  $h_{1,2}$  is shown in Equation (71) and is determined using the sine rule to find the hypotenuse of a right angled triangle used to find  $h_{1,2}$ .

$$h_{1,1} = \tan(\theta_{noz})d \quad (70)$$

$$h_{1,2} = \cos(\theta'_v - \theta') \frac{\sin(\frac{\pi}{2} - \theta'_v) \tan(\theta) X}{\sin(\theta')} \quad (71)$$

Substituting equations for  $h_{1,1}$  and  $h_{1,2}$  into Equation (69) results in Equation (72), jet-valve impact velocity as a function of  $\theta$ .

$$v = \left( v_{noz}^2 + 2 * 9.81 \left( \tan(\theta_{noz})d + \cos(\theta) \frac{\sin(\frac{\pi}{2} - \theta'_v) \tan(\theta) X}{\sin(\theta'_v - \theta)} \right) \right)^{0.5} \quad (72)$$